

The effects of subduction termination on the continental lithosphere: Linking volcanism, deformation, surface uplift, and slab tearing in central Anatolia

Jonathan R. Delph^{1,*}, Bizhan Abgarmi², Kevin M. Ward^{1,3}, Susan L. Beck¹, A. Arda Özacar², George Zandt¹, Eric Sandvol⁴, Niyazi Türkelli⁵, and Doğan Kalafat⁵

¹Department of Geosciences, University of Arizona, 1040 E. 4th Street, Tucson, Arizona 85721, USA

²Geological Engineering Department, Middle East Technical University, Üniversiteler Mah. Dumlupınar Blv. No:1, Çankaya, Ankara 06800, Turkey

³Department of Geology and Geophysics, University of Utah, 115 S. 1460 E., Salt Lake City, Utah 84112, USA

⁴Department of Geological Sciences, University of Missouri, 101 Geology Building, Columbia, Missouri 65211, USA

⁵Department of Geophysics, Boğaziçi University (KOERI), Çengelköy, İstanbul 34684, Turkey

ABSTRACT

Subduction beneath central Anatolia represents the transition between continuous subduction along the Aegean trench in the west and slab break-off and/or subduction termination at the Arabian-Eurasian collision zone in the east. Using recently collected seismic data from the Continental Dynamics–Central Anatolian Tectonics project alongside a newly developed approach to the creation of a 3D shear-velocity model from the joint inversion of receiver functions and surface-wave dispersion data, we can gain important insights into the character of the downgoing, segmenting African lithosphere and its relationship with the overriding Central Anatolian plate.

These results reveal that the mantle lithosphere of central Anatolia is thin and variable (<50–80 km) due to the decoupling of the crust of accreted lithospheric blocks from their associated lithospheric mantle, which continued to subduct and was subsequently removed by slab delamination during early-mid Miocene times. The resulting lithospheric thickness variations appear to control deformation as well as the distribution of volcanism throughout the region. In the Central Anatolian Volcanic Province, the uppermost mantle is characterized by very slow shear velocities (<4.2 km/s) consistent with the presence of melt in the uppermost mantle. The fastest shear velocities observed in this study (>4.5 km/s) underlie the Central Taurus Mountains, which have experienced ~2 km of uplift in the past ~8 m.y. These velocities are consistent with lithospheric mantle, and we interpret that the recent uplift of these mountains is due to a rebound of the subducting slab after slab break-off and/or fragmentation rather than asthenospheric influx.

*Now at Department of Earth Science, Rice University, 6100 Main Street, Houston, Texas 77005, USA

INTRODUCTION

The tectonic implications of ocean-basin closure are ill defined, despite being a crucial part of the Wilson Cycle in plate tectonics (Wilson, 1968). This process is currently taking place in the Mediterranean region, where convergence between the African and Eurasian plates is leading to the termination of subduction and final closure of the long-lived Tethyan Ocean as part of the ~15,000-km-long Alpine-Himalayan orogenic belt (Lister et al., 2001). The Anatolian region is a complex zone of deformation that is centrally located in this extensive orogenic belt. In the east, complete oceanic closure was accomplished at the Arabia-Eurasia collision zone in the early Miocene (Okay et al., 2010), while continuous subduction of old Neotethyan lithosphere is still taking place along the Aegean trench in the west (Granot, 2016; Fig. 1). Central Anatolia represents a transition between these end-member processes, making it an ideal place to study the tectonic interactions between the overriding and subducting plates during the terminal stages of subduction.

Deformation within the Anatolian plate is intimately tied to the behavior of subducting African lithosphere along its southern margin. In the west, slab rollback along the Aegean trench is imposing some of the highest observed extensional strain rates in the world (Le Pichon and Kreemer, 2010) above a seemingly coherent subducting plate (Spakman et al., 1993; Piromallo and Morelli, 2003; Biryol et al., 2011), while at the Arabia-Eurasia collision zone in the east, evidence for an underthrusting slab is largely absent below the third largest orogenic plateau on Earth (the East Anatolian Plateau, Keskin, 2003; Şengör et al., 2003). Between these regions lies central Anatolia, where the character of the subducting slab is enigmatic due to a lack of a laterally continuous Wadati-Benioff zone and the fragmented appearance of the slab from tomographic images (Biryol et al., 2011). This subduction is further complicated by the arrival of attenuated Gondwanan continental lithosphere at the Cyprean trench (Schattner, 2010; Granot, 2016). These observations indicate that a recent transition from oceanic subduction to passive margin underthrusting has occurred in central Anatolia.

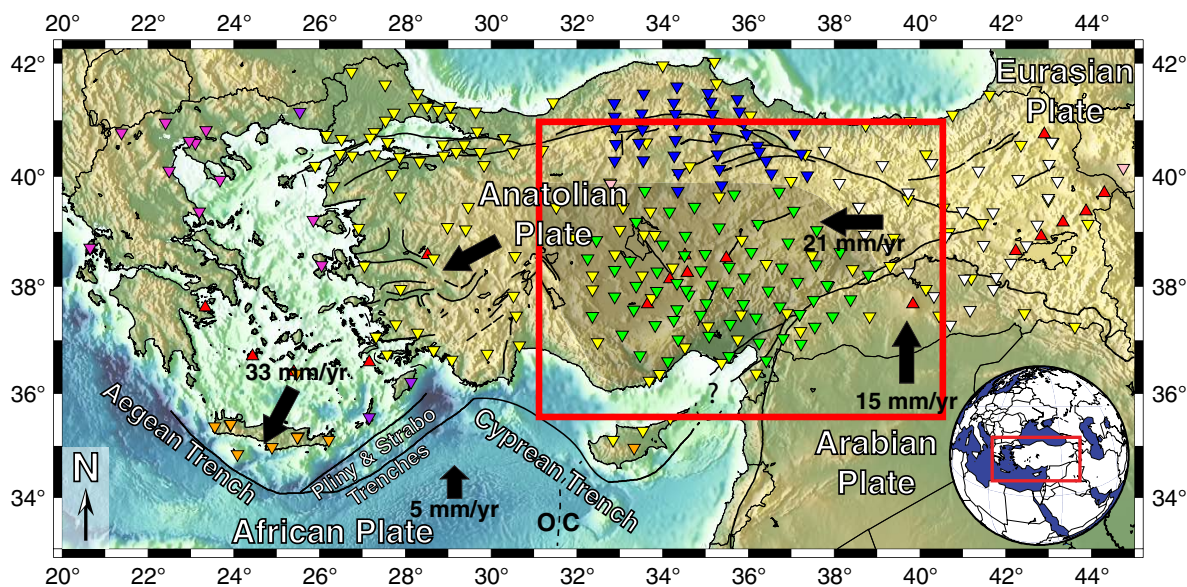


Figure 1. Map of stations used for ambient noise tomography (all) and two plane-wave tomography (green). The shaded region is what we refer to as “central Anatolia,” defined in the south by the southern margin of Anatolia, in the east by where the East Anatolian fault zone becomes a relatively discrete boundary, in the north as the region not significantly deformed by the North Anatolian fault zone, and in the west by the Isparta Angle. Black lines are major neotectonic structures and plate boundaries with southern margin boundary from Özbakir et al. (2017); red triangles are Quaternary volcanic centers. The red square outlines study area in Figure 2. Plate motion velocities are relative to Eurasia (Reilinger et al., 2006). The dashed line near the Cyprean trench represents the transition between oceanic (O) and attenuated continental (C) crust in the eastern Mediterranean (Granot, 2016).

Symbol	Experiment	Network	# Stations	Data Range
▽	Eastern Turkey Seismic Experiment	XG	29	1999-2001
▼	North Anatolian Fault Experiment	YL	39	2006-2008
▼	Kandilli Observatory Digital Broadband Network	KO	119	1999-2001, 2006-2008, 2012, 2013-2015
▼	National Observatory of Athens Digital Broadband Network	HL	3	2007-2008, 2012
▽	Global Seismographic Network	IU	2	1999-2001, 2006-2008, 2012
▼	Aristotle University of Thessaloniki Seismological Network	HT	11	2006-2008, 2012
▼	MEDNET Project	MN	1	1999-2001, 2006-2008, 2012
▼	GEOFON	GE	11	1999-2001, 2006-2008, 2012
▼	Central Anatolian Tectonics	YB	67	2013-2015
	Total	9	282	~10 years

To better understand the relationship between the tectonics of central Anatolia and the character of subduction along its southern margin, a dense array of 64 broadband seismic instruments was deployed at 72 locations as part of the Continental Dynamics–Central Anatolian Tectonics (CD-CAT) project. These stations were operational for a two-year period (May 2013–May 2015) and span the boundaries between the Anatolian, Eurasian, and westernmost Arabian plates, providing unprecedented spatial sampling throughout the region. In this study, we jointly invert P-wave receiver functions (Abgarmi et al., 2017) with Rayleigh-wave dispersion data derived from ambient noise cross correlations and earthquakes to obtain a high-resolution model of the shear-wave velocity structure beneath central Anatolia

down to ~150 km. These new seismic images will provide information about the fine-scale interactions between the underthrusting African lithosphere and the over-riding lithosphere of the Anatolian plate.

■ A MODEL FOR THE EVOLUTION OF CENTRAL ANATOLIA

The Anatolian region comprises various continental fragments that have undergone a complex history of amalgamation related to the closure of the Tethyan Ocean system (Şengör and Yılmaz, 1981; Bozkurt, 2001; Whitney and Hamilton, 2004). Colli-

sion of the Arabian plate in the east and slab rollback along the Aegean trench in the west have led to the formation of the conjugate strike-slip North and East Anatolian fault zones, which exemplify “tectonic escape” (Fig. 1) (Şengör et al., 1985; Burke and Şengör, 1986). These plate-bounding fault zones allow the Anatolian plate to translate westward and rotate counterclockwise (with respect to fixed Eurasia) as a coherent unit in a regional sense (Reilinger et al., 2006). The apparent coherency of this tectonic block, however, does not imply simplicity in the tectonic structures that have been imposed by the long-lived evolution of the Tethyan Ocean and the recent dynamics of the convergent margin.

The Late Cretaceous–Early Tertiary evolution of central Anatolia can be summarized by the closure of the northern branch of the Neotethys Ocean along the south-vergent Late Cretaceous–Paleocene Izmir-Ankara-Erzincan suture zone (IAESZ) and Inner-Tauride suture (ITS) (Şengör and Yılmaz, 1981; Boztuğ et al., 2009; Parlak et al., 2013). The accretion of continental material (namely, the Kirşehir and Anatolide-Tauride blocks; Fig. 2 inset) onto the southern margin of Eurasia as crustal-scale nappe complexes was accommodated by detachment and decoupling of the crust from the underlying mantle lithosphere (Bartol and Govers, 2014; van Hinsbergen et al., 2016). This has led to a continuous southward migration of the trench from the Eocene to present (Menant et al., 2016; van Hinsbergen et al., 2016). However, the mantle lithosphere of the subducting plate may have continued to underthrust at a relatively shallow angle during the Eocene–Oligocene (Bartol and Govers, 2014). Shortly thereafter, the subducting slab began to founder from the overriding plate, leading to extension in the upper plate as evidenced by the

early-mid Miocene unroofing of metamorphic core complexes in the Kirşehir Block (Fayon and Whitney, 2007). Foundering was likely caused by a decrease in the convergence rate between Africa and Eurasia, as indicated by the development of backarc basins and trench migration throughout the entire Mediterranean region (Jolivet and Faccenna, 2000). The presumably thin lithosphere of the Central Anatolian region was then exposed to hot upwelling asthenospheric material that adiabatically melted and initiated large ignimbritic eruptions beginning in the mid-Miocene (Le Pennec et al., 1994; Aydar et al., 2012). The subducting slab appears to have foundered in the southwestward direction in central Anatolia, as indicated by the southwest-younging of the initiation of volcanism in the Central Anatolian Volcanic Province (Schleiffarth et al., 2015) and NE-SW-oriented shear-wave splitting orientations in Anatolia (Paul et al., 2014 and references therein). In the late Miocene, the initiation of the uplift of nearly flat-lying carbonates in the Central Taurus Mountains is interpreted to result from slab fragmentation and subsequent rebound in the downgoing plate (Duretz et al., 2011; Schildgen et al., 2014). In Pliocene to younger times, subduction has been further complicated by the arrival of Gondwanan-derived continental fragments along the southern margin of Anatolia (e.g., Schattner, 2010; Delph et al., 2015a). This underthrusting of attenuated continental material has led to an acceleration in the uplift rate of the Central Taurus Mountains (Schildgen et al., 2012) and an apparent change in dip of the Cyprian slab from W to E (Biryol et al., 2011); this change in dip corresponds well with the inferred boundary between subducting oceanic and continental material in the Eastern Mediterranean (Granot, 2016).

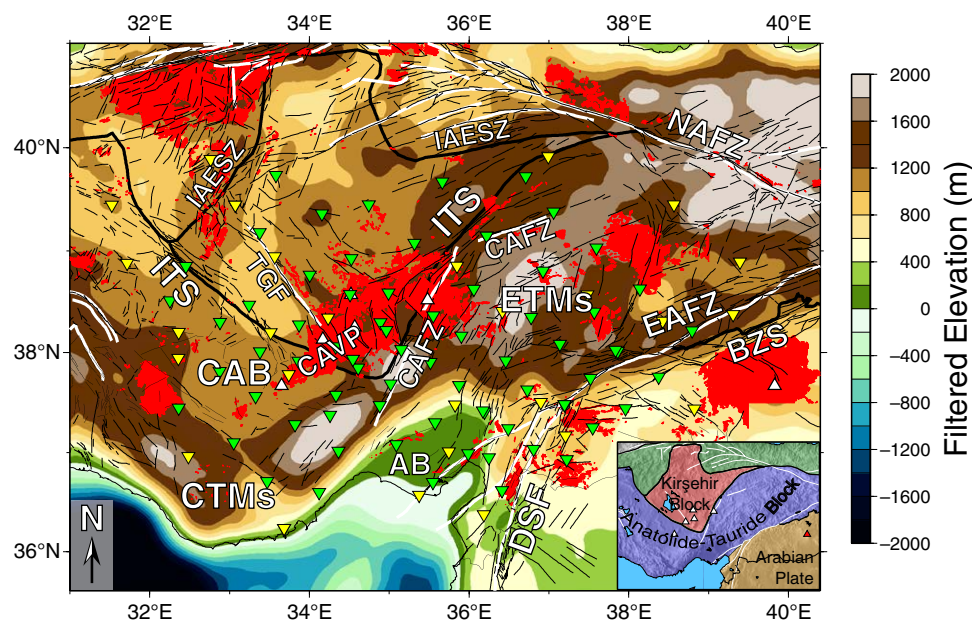


Figure 2. Smoothed topography of central Anatolia (50 km spatial smoother). The elevated regions (dark brown to white) approximately delineate the Taurus Mountains. A sharp transition to lower elevations occurs along the Inner-Tauride suture (ITS) between the Taurus Mountains and the Kirşehir Block. Red polygons represent Miocene to recent volcanics, thick black lines are sutures, thin black lines are minor neotectonic faults, and white lines are major faults. Green inverted triangles are Continental Dynamics–Central Anatolian Tectonics (CD-CAT) stations used in two plane-wave tomography and yellow inverted triangles are Kandilli Observatory and Earthquake Research Institute (KOERI) stations used with CD-CAT stations in the receiver-function analysis (Abgarni et al., 2017). Inset shows relevant geologic terranes. AB—Adana Basin; BZS—Bitlis-Zagros suture; CAB—Central Anatolian Basin; CAFZ—Central Anatolian fault zone; CAVP—Central Anatolian Volcanic Province; CTMs—Central Taurus Mountains; DSF—Dead Sea fault; EAFZ—East Anatolian fault zone; ETMs—Eastern Taurus Mountains; IAESZ—Izmir-Ankara-Erzincan suture zone; ITS—Inner-Tauride suture; NAFZ—North Anatolian fault zone; TGF—Tuz Gölü fault.

■ GEOLOGIC AND TECTONIC BACKGROUND

Geologic Terranes

Two main geologic terranes comprise our study area: the Kirşehir Block and the Anatolide-Tauride Block (Fig. 2). The basement of the Kirşehir Block consists primarily of crystalline metamorphic and plutonic rocks of island-arc affinity as well as obducted ophiolitic fragments (Whitney et al., 2001; Lefebvre et al., 2015). This domain is bounded in the north and south by the Izmir-Ankara-Erzincan suture zone (IAESZ) and Inner-Tauride suture (ITS) (Okay and Tüysüz, 1999; Parlak et al., 2013). The Inner-Tauride suture is thought to mark the closure of a small Neotethyan ocean basin that separated the Anatolide-Tauride Block from the Kirşehir Block (van Hinsbergen et al., 2016) and correlates with the surficial location of a drastic change in geophysical properties, including Bouguer gravity anomalies (Ates et al., 1999), Pn velocity (Gans et al., 2009; Mutlu and Karabulut, 2011), phase velocities from ambient noise tomography (Warren et al., 2013; Delph et al., 2015a), and crustal thickness (Abgarmi et al., 2017). The Anatolide-Tauride Block originated on the Gondwanan passive margin. In central Anatolia, it generally consists of unmetamorphosed marine sedimentary rocks where exposed (Cosentino et al., 2012) and is separated from the Kirşehir Block by the sedimentary basins of the Tuz Gölü, Konya, and Ulukışla basins (hereafter referred to as the central Anatolia Basin based to their similarities in velocity structure; however, this grouping does not imply that the evolution of these basins is related). The Anatolide-Tauride Block becomes more heavily deformed in the Eastern Taurus Mountains across the Central Anatolian fault zone due to stresses imposed by the northward motion of the Arabian plate.

The Central Anatolian Fault Zone

The ~730 km Central Anatolian fault zone is a seismically active, transtensional structure dominated by low-magnitude events and low rates of lateral displacement (no more than 80 km total and only ~2–3 km since 13 Ma; Koçyiğit and Beyhan, 1998) that demarcates the transition between transpressional deformation to the east and transtension to the west and largely exploits the lithospheric weakness associated with the eastern Inner-Tauride suture. Deformation in the central portion of the Central Anatolian fault zone (Ecemiş corridor) has become largely extensional since the late Pliocene, leading to the formation of a pull-apart basin that is home to the northern portion of the Central Anatolian Volcanic Province (Toprak, 1998; Higgins et al., 2015).

The Central Anatolian Volcanic Province

The Central Anatolian Volcanic Province is a NE-SW-trending, long (~300 km) and broad (40–100 km) volcanic region comprising voluminous felsic-intermediate ignimbrite deposits (>1000 km³; Le Pennec et al., 1994), large polygenetic stratovol-

canoes, and smaller monogenetic cones and domes that correlate with inherited deformational structures near the Central Anatolian fault zone and Inner-Tauride suture (Toprak and Göncüoğlu, 1993; Toprak, 1998; Aydın et al., 2014). Ignimbrite volcanism in the region began in the mid-late Miocene (Aydar et al., 2012) and is concentrated near the projected junction of the Tuz Gölü fault and Central Anatolian fault zone at the buried transition from the Kirşehir Block to the Anatolide-Tauride Block. This large-volume ignimbrite volcanism gives way to smaller, more mafic eruptions to the south in the Anatolide-Tauride Block. The initiation of volcanism in the Central Anatolian Volcanic Province also appears to show a southwestward-younging trend (Schleiffarth et al., 2015).

The Central Taurus Mountains

Bounding the southern edge of the Central Anatolian Volcanic Province and Central Anatolian Basin are the Central Taurus Mountains. The Central Taurus Mountains have experienced multiple phases of uplift since the late Miocene: the first ca. 8 Ma, interpreted as a result of slab break-off, and the second beginning ca. 1.6 Ma, contemporaneous to the arrival of the Eratosthenes seamount at the Cyprean trench (Cosentino et al., 2012; Schildgen et al., 2012). These processes are interpreted to have caused a cumulative uplift of ~2 km in the absence of significant compressional deformation as evidenced by nearly flat-lying Miocene shallow-marine carbonates that lie atop much of the Central Taurus Mountains. Upwelling asthenosphere as a result of slab break-off has been proposed to be responsible for this dramatic uplift (Cosentino et al., 2012); however, recent geophysical imaging of upper-mantle structure in central Anatolia indicates that the Cyprean slab may be present as far north as the northern margin of the Central Taurus Mountains (Bakırcı et al., 2012; Abgarmi et al., 2017).

The Bitlis-Zagros Suture

The Bitlis-Zagros suture formed as a result of the final closure of the Neotethyan Ocean between Arabia and Eurasia in the early Miocene (Okay et al., 2010). Today, it represents the boundary between the Anatolian and Arabian plates in the west and Eurasian and Arabian plates in the east. The western portion of the Bitlis-Zagros suture roughly delineates the location of the long (~500 km), broad (~20 km), and very seismically active East Anatolian fault zone (EAFZ) (Bulut et al., 2012). In the Adana Basin, the EAFZ branches into multiple strands and transitions from dominantly left-lateral strike-slip motion to transtension, marking a diffuse plate boundary resulting from a compatibility gap at a continental triple junction (Dewey et al., 1986). This has led to drastic crustal thinning beneath the Adana Basin, a steep gradient in crustal thicknesses (Abgarmi et al., 2017), and differential uplift rates across the Kozan fault, which separates the Adana Basin from the Central Taurus Mountains (Radeff et al., 2015).

METHODS

Ambient Noise Tomography

In this study, we add an additional two years of seismic data (May 2013–May 2015) from ~170 stations from the recent CD-CAT seismic deployment and the Kandilli Observatory and Earthquake Research Institute (KOERI) to the data set of Delph et al. (2015a) (Fig. 1). The seismic portion of the CD-CAT project involved the deployment of 64 broadband seismic stations (STS-2 and CMG-3T sensors) in 72 locations throughout central Anatolia.

We perform ambient noise tomography on this new data set following the method of Bensen et al. (2007). The addition of the CD-CAT data set nearly doubles the number of raypaths that sample the Anatolian region from Delph et al. (2015a) while adding significant data coverage to the central portion of Anatolia. We first remove the trend, mean, and instrument responses from all vertical-component data and filter between the periods of 5–150 seconds so that consistent measurements of ground motion can be cross correlated for all contemporaneously recording seismic stations. These interstation cross correlations are then stacked over the duration of operation to increase their signal-to-noise ratio (SNR), and the positive and negative time lags of the cross correlations are averaged to obtain waveforms that represent surface (Rayleigh) waves traveling between stations. Waveforms with a SNR ≥ 10 are analyzed using frequency-time analysis (FTAN) to estimate interstation Rayleigh-wave phase velocities (Bensen et al., 2007). Recent research has shown that accurate Rayleigh-wave measurements can be obtained at a station spacing ~ 1 wavelength, contrary to the assumption that an interstation spacing of at least 3x wavelength was necessary to accurately recover surface-wave velocities (Luo et al., 2015). This significantly increases the number of useable interstation phase velocities recorded by the CD-CAT array. These interstation phase velocities are then inverted for phase-velocity maps as a function of period (from 8 to 50 seconds) using the tomographic method of Barmin et al. (2001) with damping and smoothing parameters of 300 and 50 km. These parameters are chosen based on a trade-off plot of the root-mean-square (RMS) travel-time residual and the trace of the smoothing term in the inversion matrix normalized by the size of the smoothing matrix (Fig. 3A). The smoothing parameter is slightly smaller than that used in Delph et al. (2015a) as justified by the trade-off plot and the very dense ray coverage after the introduction of the CD-CAT data (Fig. 3A). This inversion also incorporates a ray-density-dependent weighting parameter that controls velocity variations in areas of poor ray density. Variation

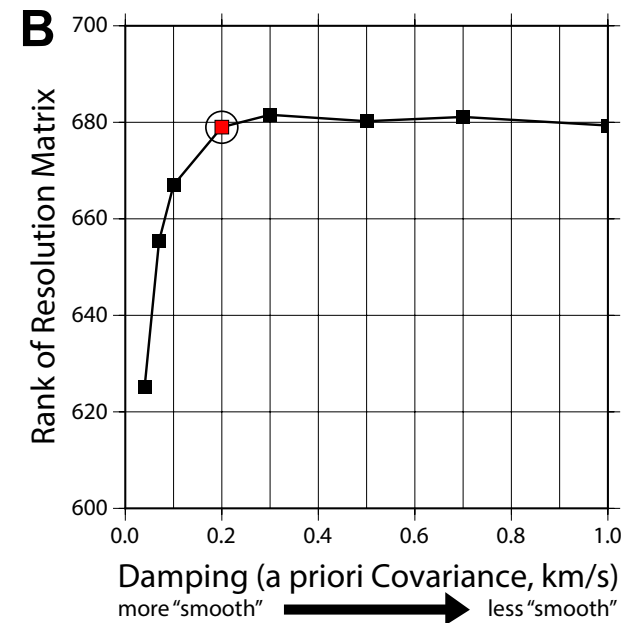
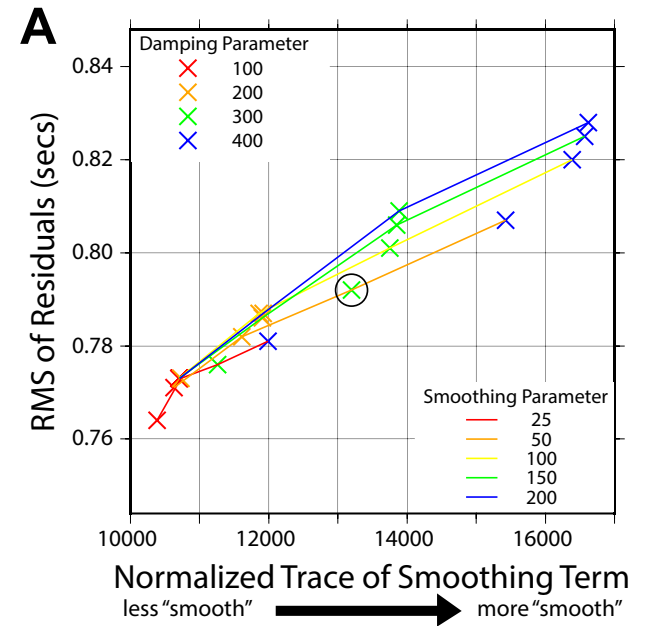


Figure 3. (A) Trade-off plot of model fit to travel times as a function of the smoothing and damping parameter for the inversion of ambient noise phase velocities at 20 seconds (Barmin et al., 2001). Y-axis is the final root-mean-square (RMS) travel-time residual. A good balance of fit to the data and model smoothness is sought, which we find at a damping of 300 and smoothing kernel of 50 km. This relationship holds at all periods for which we obtained ambient noise results. (B) Trade-off plot of initial model covariance, which acts as a damping parameter, and trace of the resolution matrix for the two plane-wave inversion for 50-second earthquake-generated Rayleigh waves. A covariance of 0.2 km/s allows for the largest variation while keeping the model from having unrealistic, high-amplitude anomalies. The smoothing parameter is set to 50 km to be consistent with the ambient noise tomography inversion.

of this parameter has a relatively small effect on the resulting phase-velocity maps when applied to this ambient noise data set due to the very dense sampling of our study area, and we use a value of 100 for this study.

Two Plane-Wave Tomography

Two plane-wave tomography (TPWT; Forsyth and Li, 2005) has proven to be a powerful way to obtain surface-wave dispersion information with a distributed array. TPWT models an incoming surface wave as two interfering plane waves described by amplitude, phase, and direction to account for lateral velocity heterogeneities and scattering outside of the array, which can cause the incoming ray path to deviate from the great-circle path between the earthquake and array. To fully describe the different lateral sensitivities of the Rayleigh waves used in this study, finite frequency sensitivity kernels using the Born single-scattering approximation are used; these kernels allow for the accurate recovery of anomalies as small as ~ 1 wavelength at the period of interest (Zhou et al., 2004; Yang and Forsyth, 2006). Since this research focuses on central Anatolia, we perform TPWT only on the CD-CAT stations.

For this data set, we inspect $M_w \geq 6$ earthquakes at 25° – 125° epicentral distances from our station locations on vertical 1 sample/second waveform data. First, we removed the trend, mean, and instrument responses of all stations to ensure data are in a common unit (displacement). After discarding all traces where an earthquake was not easily observable, we perform a narrow bandpass filter with a 10 mHz filter width centered at 13 frequencies with periods corresponding to 25–143 seconds. High-quality Rayleigh-wave arrivals were then windowed and used for TPWT. Periods < 40 seconds returned an insufficient number of high-quality Rayleigh waveforms and were omitted from further analysis, as most of the higher frequency content of the Rayleigh waves had attenuated due to the large epicentral distances of the earthquakes in this study ($> 70^\circ$) (Fig. 4). Some longer periods were also excluded (125 and 143 seconds) because the wavelength of the Rayleigh waves at these periods surpassed the spatial dimensions of the seismic array, compromising the accuracy of the phase-velocity measurements (Fig. 5) (Yang and Forsyth, 2006). However, the 111 second phase-velocity measurement was retained because it could still recover the pattern of anomalies, albeit with underestimated amplitudes (Supplemental Fig. S1¹). The TPWT model region extends beyond our array so that nodes outside of the array can absorb velocity heterogeneities from scattering outside of the footprint of the seismic array.

Because the two plane-wave inversion is a smoothed, damped least-squares inversion, it is important to have an initial phase-velocity model that is close to the real phase-velocity structure of the study region (Rau and Forsyth, 2011). To account for vertical and lateral variations in crustal-velocity structure, we follow the method described by Delph et al. (2015a) to obtain a simple 3D shear-velocity model from ambient noise tomography (ANT)-derived dispersion data using an updated compilation of crustal thickness estimates for the Anatolian region (Supplemental Fig. S2 [see footnote 1]) (Özacar et al., 2010; Vanacore et al., 2013; Abgarmi et al., 2017). Below the crust, we append a constant-velocity mantle of $V_s = 4.3$ km/s based on the

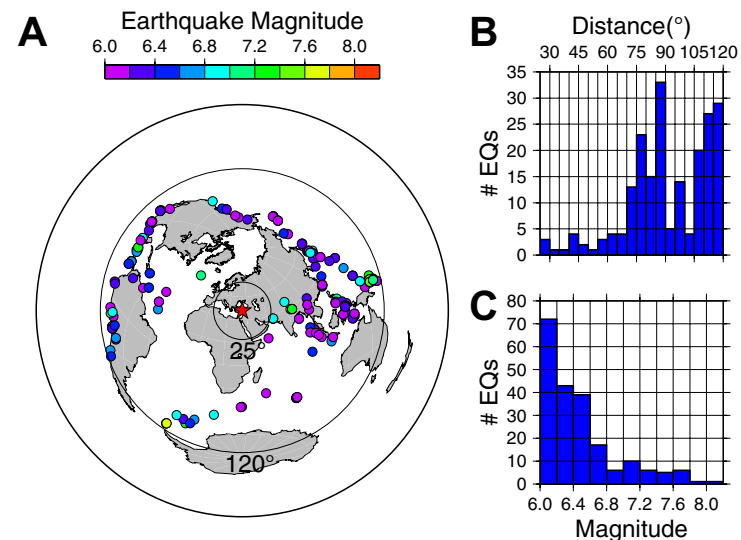


Figure 4. (A) Map of earthquake distribution used in this study. (B) Histogram of earthquakes as a function of distance. The dominant sources of earthquakes are from South America and the western Pacific. The large epicentral distances combined with high attenuation in the Anatolian region makes it difficult to measure short-period (< 40 s) Rayleigh waves generated by earthquake sources. (C) Histogram of earthquakes as a function of magnitude.

average shear velocity in the upper mantle beneath Anatolia (Fichtner et al., 2013; Delph et al., 2015a). Dispersion data from this 3D shear-velocity model was then calculated to produce a starting model of Rayleigh-wave phase velocities at different periods (40, 45, 50, 59, 67, 77, 91, 100, and 111 seconds) for the two plane-wave inversions. Other mantle velocities were tested as well, but these did not change the inverted phase-velocity maps by more than ~ 50 m/s.

The two plane-wave inversion is dependent on a spatial smoothing and damping parameter to stabilize anomalies within the model area. For spatial smoothing,

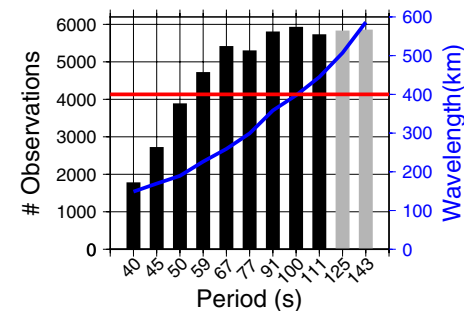
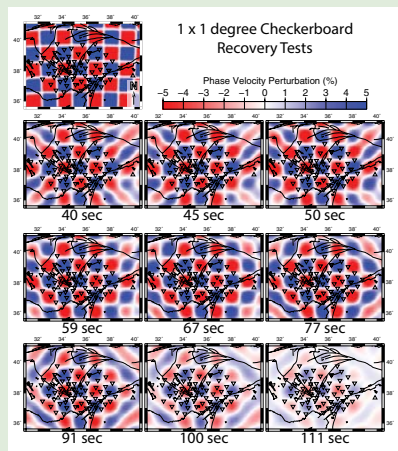


Figure 5. Number of observations used in the two plane-wave tomographic inversion for each period. Longer periods show significantly higher-quality events. At periods ≥ 111 seconds, the average wavelength of a Rayleigh wave (blue line) is longer than the N-S spatial footprint of the array (red line), limiting the reliability and lateral resolution of anomalies at longer periods; thus, periods of 125 and 143 seconds were excluded from the shear-wave inversion.



¹Supplemental Figures. (1) Checkerboard test for 1×1 degree anomalies; (2) crustal thickness map of Anatolia used to generate starting model of phase velocities for two plane-wave inversion; (3) Mapview of NRMS joint inversion fits to receiver functions and dispersion data; and (4) two plane-wave tomography results at periods from 40–111 seconds. Please visit <http://doi.org/10.1130/GES01478.S1> or the full-text article on www.gsapubs.org to view the Supplemental Figures.

we use a similar Gaussian pulse width as used in the ambient noise tomographic inversion (50 km), which acts to smooth the sensitivity kernels estimated from the Born approximation. This smoothing parameter has a much greater effect on short-period kernels than those of longer periods (see Li, 2011, fig. 3, for example). We choose a damping parameter of 0.2 because the rank of the resolution matrix stabilizes at this value (Fig. 3B). Our grid spacing is set at $0.2^\circ \times 0.2^\circ$ to match that of the ambient noise tomography grid.

This inversion is a two-step process for which we perform three iterations at each step. In the first step, the inversion solves for the amplitude, phase, and direction of two interfering plane waves that best reproduce the windowed waveforms from each event using a simulated annealing approach. In the second step, phase velocities are estimated using the observed and predicted arrival times of the waveforms based on the best-fitting wave parameters from the first step, which can be further adjusted in this step to better fit the waveforms (Forsyth and Li, 2005; Yang and Forsyth, 2006). With the data and inversion parameters used in this study, we were able to resolve anomalies of $1^\circ \times 1^\circ$ at all periods investigated based on checkerboard tests (Supplemental Fig. S1 [see footnote 1]). Due to the increasing wavelength as a function of period, shorter period measurements are able to resolve smaller-scale structures enabling accurate recoveries of lateral gradients in phase-velocity structure, while longer periods (>91 seconds) accurately recover the pattern of the anomalies smaller than $1^\circ \times 1^\circ$ but with diminished amplitudes.

The Joint Inversion of Multiple Data Sets

By combining receiver functions derived from common conversion point (CCP) stacking (Dueker and Sheehan, 1997) with ANT-derived dispersion data, a high-resolution shear-wave velocity model can be obtained for the crust and uppermost mantle (Julià et al., 2000; Delph et al., 2015b; Delph et al., 2017). In this study, we build on this approach by combining longer period dispersion data obtained through TPWT to obtain shear-wave velocity results deeper into the upper mantle. Rayleigh waves at periods obtained from earthquake sources (generally >20 seconds) have very little sensitivity to upper-crustal structure, and thus it is important to pair them with shorter period data from ANT to better constrain crustal-velocity structure. By utilizing the joint inversion of receiver functions and ANT-derived dispersion data, we can obtain a crustal model that mitigates the need to assume an a priori crustal model that may be weakly constrained.

We follow the methodology described by Delph et al. (2015b) and Delph et al. (2017) to create CCP-derived receiver functions. First, we re-compute the high-quality receiver functions obtained by Abgarmi et al. (2017) using a Gaussian low-pass filter of ~ 1.4 Hz (Gaussian pulse with a 2.8 alpha parameter). We then compute a CCP volume with bin spacing of 0.2° and a minimum bin width of 0.3° that can dilate until a minimum of 10 rays is incorporated into the bin or a bin width of 1° is reached. This approach creates a laterally smoothed and gridded 3D model of conversion amplitudes in the Earth. The receiver functions in this analysis are migrated with a two-layer velocity model consisting of crustal and mantle shear velocities of 3.4 km/s and 4.2 km/s with a V_p/V_s ratio of 1.78, which is representa-

tive of the average structure in central Anatolia (Delph et al., 2015a). This velocity model has a minimal effect on the resulting CCP-derived receiver functions, as the same velocity model is used to migrate the newly stacked receiver functions back to time (Delph et al., 2015b). A Gaussian filter is then used on the resulting CCP profiles to reduce the effects of spurious and unrealistic amplitude artifacts, which result from introducing new data into a CCP bin (see Delph et al., 2017, for details). The end result is equivalent to a P-wave receiver function filtered with a 1.2 Hz Gaussian (2.5 alpha parameter, ~ 1 km vertical resolution) at each grid point. This receiver function can then be paired with a surface-wave dispersion measurement for the joint inversion.

To prevent inverting receiver-function multiples generated from the crust-mantle boundary (PpPs and PsPs + PpSs, respectively), we invert only the first 8 seconds of the receiver function (sensitive to depths <65 km). At depths greater than 65 km, only Rayleigh-wave dispersion data are used in the inversion for shear velocities. Because of the broad sensitivity kernels of Rayleigh waves (e.g., Fig. 6B), we increase our model layer thickness so that the diagonal of the resolution matrix is >0.1 with respect to the dispersion data. With the dispersion data used in this study, we can obtain shear-wave velocities down to ~ 150 km (Figs. 6B and 7A). In order to create a smoothed, continuous volume of shear-wave velocities in the upper mantle where layers are thick, we perform a cubic interpolation between layer velocities for every depth profile. The resulting profile honors all layer velocities and does not significantly degrade fit to the dispersion data. Some of the stations of Abgarmi et al. (2017) were omitted from this analysis due to complicated waveforms at times corresponding to shallow crustal depths that cannot be adequately modeled by the joint inversion algorithm. Gaps in the resulting 3D model were filled using a linear interpolation between nearby data points for each layer. There were no gaps more than 0.4° away from any data point constrained by the joint inversion, and these gaps were largely focused in the western Central Anatolian Basin (see Supplemental Fig. S3 [footnote 1] for fits to data sets and gap locations).

RESULTS

Phase-Velocity Results

The new ambient noise tomography model that incorporates two years of CD-CAT and KOERI seismic data is similar to the ambient noise tomography data set of Delph et al. (2015a), with slightly faster phase velocities beneath the Central and Eastern Taurus Mountains at longer periods (>30 seconds). At periods where both ANT and TPWT obtain phase-velocity results (40, 45, and 50 seconds), the two methods return values consistent with each other (within ~ 0.05 km/s on average; Table 1).

Phase velocities from TPWT and ANT at all periods are slow throughout most of central Anatolia relative to the global model AK135 (Fig. 6; Fig. 8A, anomaly 1). Dispersion curves from ANT and TPWT in the Arabian plate (AP), the Eastern Taurus Mountains, the Central Taurus Mountains, and the Central Anatolian Basin are shown in Figure 6 (locations are shown as colored stars in Fig. 8D). Beneath the

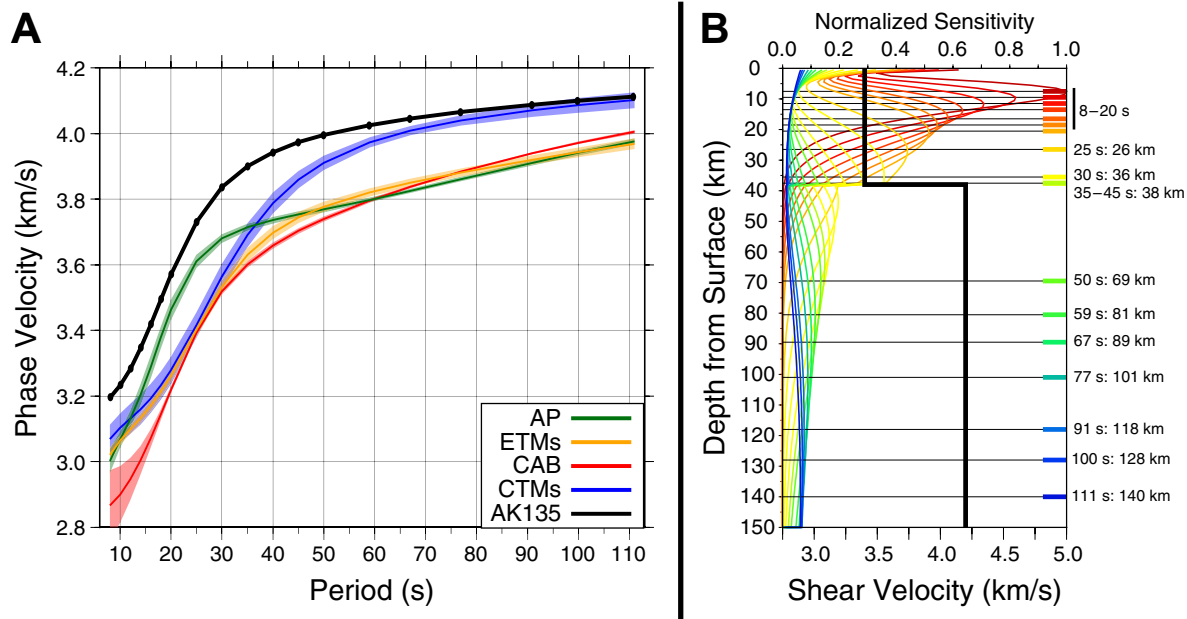


Figure 6. (A) Phase-velocity dispersion curves (solid) and standard deviations (shaded) from the inverted shear-velocity model for a $0.6^\circ \times 0.6^\circ$ area centered in different tectonic regions (center locations shown in Fig. 8D). Most of Anatolia is slower than global-velocity model dispersion data (black line). Low velocity gradients at short (<30 second) periods indicate slow seismic velocities that could correspond to regions of thick crust or slow upper-mantle velocities. Relatively fast phase velocities at intermediate periods beneath the Central Taurus Mountains are indicative of seismically fast material in the upper mantle. AP—Arabian plate; ETMs—Eastern Taurus Mountains; CAB—Central Anatolian Basin; CTMs—Central Taurus Mountains. (B) Sensitivity kernels for different Rayleigh-wave periods based on a simplified shear-velocity model derived from Delph et al. (2015a) in black. Phase velocities are a result of the depth-integrated sensitivity of the individual kernels. The depth to the peak sensitivity of each period is shown on the right.

northwestern Arabian plate, phase velocities are indicative of a thin crust and fast uppermost mantle as seen by the steep increase in phase velocities at short periods (green) (Fig. 6A; Supplemental Fig. S4 [see footnote 1]). At longer periods, phase velocities beneath the northern Arabian plate are similar to those in the Eastern Taurus Mountains and the Central Anatolian Basin, indicating that deeper mantle shear velocities in both regions may be similar. The slow phase velocities in the shortest periods (<20 seconds) for the Central Anatolian Basin are most likely due to the presence of thick sedimentary deposits. These phase velocities remain slow at periods sensitive to upper-mantle shear-wave velocities (>20 seconds) despite the region having a thin crust. These results for the Central Anatolian Basin, along with numerous other studies (e.g., Bakırcı et al., 2012; Salaün et al., 2012; Fichtner et al., 2013; Delph et al., 2015a; Govers and Fichtner, 2016), provide consistent evidence that the shear-wave velocities of the uppermost mantle in central Anatolia are slower than typical upper-mantle velocities. The slightly faster phase velocities beneath the Eastern Taurus Mountains at intermediate periods (30–59 seconds, orange curve in Fig. 6A) indicate that the lower crust and/or uppermost mantle of the Eastern Taurus Mountains must contain seismically faster material than the nearby Central Anatolian Basin, as the crust is ~15 km thicker beneath the Eastern Taurus Mountains (Abgarmi et al., 2017). Lastly, dispersion data from the Central Taurus Mountains are consistent with a relatively thicker crust based on its low gradient at short periods. These dispersion data become much faster at intermediate and long periods (>30 seconds) compared to most of Anatolia, indicating the presence of fast lower-crustal and/or mantle shear velocities extending to significant

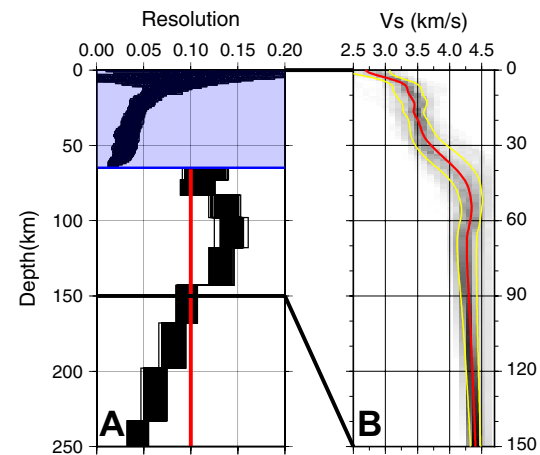


Figure 7. (A) Diagonal of the resolution matrix for the shear-wave inversion. The low values of the blue shaded region are a result of the thin layers where the joint inversion with receiver functions is used. The thin layers are necessary to allow discontinuities from the receiver functions to be placed at their proper depths. At depths >65 km, layers thicken and only dispersion data are inverted for shear-wave velocities. The region to the right of the red line is where we obtain satisfactory measurements. (B) Average shear-wave velocity of all inverted grid points (red line) and the standard deviation (yellow lines). Background color is a histogram of individual shear-wave velocity measurements, with darker colors indicating a higher number of measurements.

TABLE 1. DIFFERENCE BETWEEN TWO PLANE-WAVE TOMOGRAPHY AND AMBIENT NOISE TOMOGRAPHY RESULTS

Period	Average difference (km/s)	Standard deviation (km/s)
40	0.025	0.051
45	0.031	0.056
50	0.025	0.065

Notes: Average difference and standard deviation between Rayleigh-wave phase velocities at the same grid point derived from two plane-wave tomography and ambient noise tomography. In general, phase velocities obtained from two-plane-wave tomography are slightly faster, while the standard deviation of the differences increases with increasing periods.

depths. In fact, a fast phase-velocity anomaly underlies much of the Central Taurus Mountains (Fig. 8, anomaly 2). Abgarmi et al. (2017) proposed that the African lithosphere (or the “Cyprean slab”) was present beneath central Anatolia as far north as the northern margin of the Central Taurus Mountains based on intermediate depth (~50–70 km) conversions in receiver functions. This is consistent with fast (>4.4 km/s) shear velocities obtained from the inversion of Rayleigh-wave dispersion data (Bakırcı et al., 2012) and full-waveform tomography (Govers and Fichtner, 2016). On a regional scale, longer-period phase velocities (≥100 seconds) show very little lateral variation, with a low-magnitude relative fast velocity anomaly underlying much of central Anatolia (Fig. 8D, anomaly 3).

Shear-Wave Velocity Model

Shear-wave velocities in the crust and uppermost mantle throughout the study area are generally slow (Fig. 7B), consistent with previous studies of shear velocity in the region (Bakırcı et al., 2012; Salaün et al., 2012; Fichtner et al., 2013; Delph et al., 2015a; Govers and Fichtner, 2016). The Arabian plate can be distinguished from the Anatolian plate by its thin crust and relatively fast uppermost-mantle shear-wave velocities (>4.4 km/s) compared to the thicker crust and seismically slower uppermost mantle of the Anatolian lithosphere (Fig. 9B). Crustal thickness estimates in the Arabian plate (30–35 km) agree well with a sharp increase in shear-wave velocities from ~3.5 km/s to >4.4 km/s. These fast shear velocities extend down to ~50–60 km where they are underlain by a large negative gradient, eventually reaching shear velocities that are much slower than expected for mantle lithosphere (<4.2 km/s at ~60–110 km below the surface) (Figs. 9C, 9D, 10B, and 10D).

Farther west, there is a sharp transition from the fast velocities observed in the crust and mantle of the Arabian plate to very slow crustal shear velocities in the Adana Basin (<3.2 km/s) extending down to ~17 km (Figs. 9A and 10A). Faster shear velocities at depths ~30–60 km consistent with lithospheric mantle wave speeds extend below the eastern portion of the Adana Basin as well as locally beneath the Eastern Taurus Mountains. These fast velocities terminate to the west near the center of the Adana Basin, transitioning to slower velocities consistent with the lower crust of the Anatolian plate (Fig. 10B).

Beneath the Central Taurus Mountains and westernmost Adana Basin, we observe vertically extensive fast shear velocities (up to 4.8 km/s) beginning at a depth

of ~60 km (Figs. 9C, 9D, 10B, and 10C). These fast velocities appear to underlie much of the Central Taurus Mountains and extend as far north as the Central Anatolian Basin, where they transition rather abruptly to slow upper-mantle shear velocities. To the east, these fast velocities are separated from the fast velocities associated with the upper mantle of the Arabian plate by a narrow band of slow shear velocities that indicates that these are separate features (Fig. 10B).

Shear velocities in the upper crust of the Central Anatolian Basin are generally low (<3.4 km/s) due to the thick sedimentary deposits in the region (Fig. 9A). In the mantle, we observe the slowest shear velocities in the study area near the western edge of the Central Anatolian fault zone. These slow velocities show a NE-SW trend

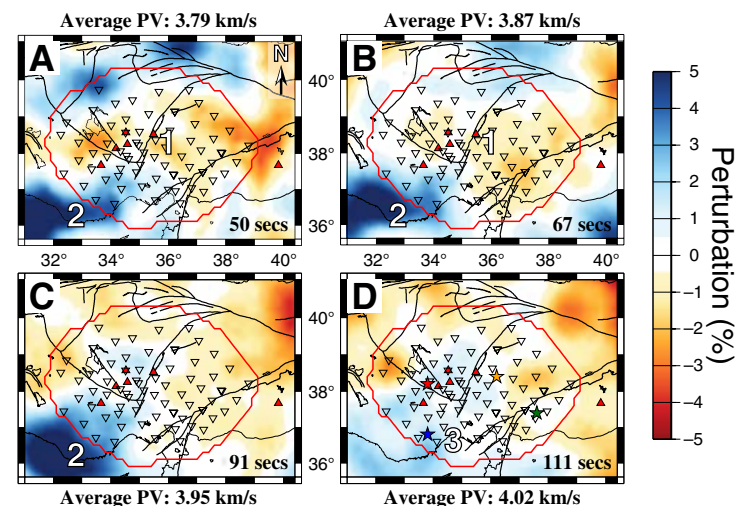


Figure 8. Phase-velocity maps at (A) 50 second, (B) 67 second, (C) 91 second, and (D) 111 second periods from two plane-wave tomography. Scale is relative to the mean for the period inside the red polygon, which approximately delineates the regions where we have reliable results. Anomaly (1) is consistent with slow seismic velocities at upper-mantle depths beneath central Anatolia. Anomaly (2) is consistent with recent interpretations that there may be a slab beneath the Central Taurus Mountains. Anomaly (3) indicates that slightly faster seismic velocities are present beneath central Anatolia at deeper (>100 km) depths relative to the surrounding region. Stars in 8D show locations of dispersion data in Figure 6A.

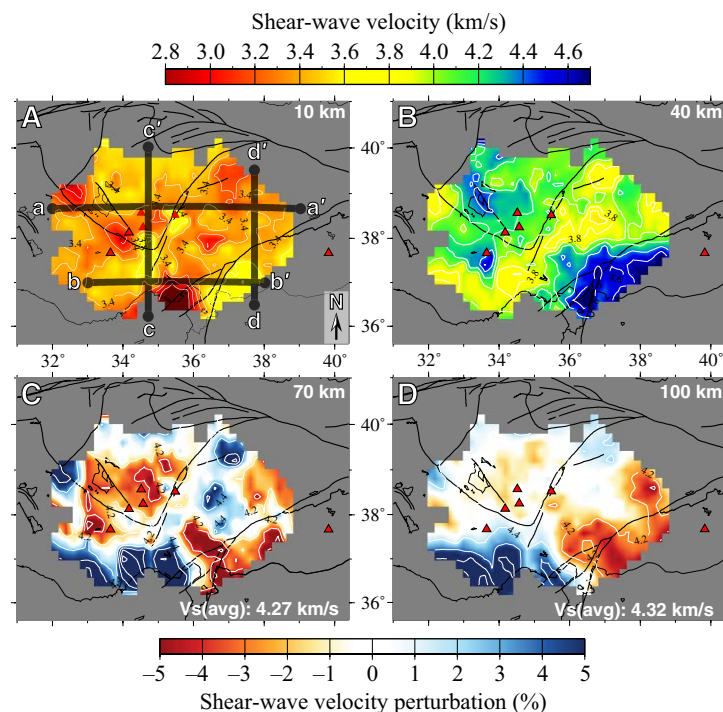


Figure 9. Depth slices relative to surface in absolute shear velocity (A and B) and shear velocities relative to the mean profile in Figure 8B (C and D). Tectonic provinces and major faults shown as black lines; red triangles are Holocene volcanoes; white contours are absolute shear velocities. (A) 10 km; slow shear velocities are observed in the Central Anatolian Basin and Adana Basin, while faster shallow velocities characterize the Taurus Mountains, Kirşehir Block, and Arabian plate. Thick black lines correspond to cross sections in Figure 10. (B) 40 km; differences between fast (>4.0 km/s) and slow (<4.0 km/s) correspond mostly to crustal thickness variations. The Taurus Mountains have thicker (>40 km) crust, while the Arabian plate has thin (<35 km) crust (Abgami et al., 2017). (C) 70 km; very slow shear velocities (<4.2 km/s) present beneath most of the Central Anatolian Basin and Central Anatolian Volcanic Province as well as below the fast mantle lithosphere of the Arabian plate. Fast shear velocities along the southern margin of Anatolia are interpreted as subducting African lithosphere. (D) 100 km; deep-seated slow velocities beneath the Arabian plate may indicate that the origin of upwelling asthenosphere that is prevalent beneath the Anatolian plate comes from the south, flowing to shallower depth in a northwesterly direction to the Central Anatolian Volcanic Province. Fast velocities beneath the southern Anatolian margin indicate the presence of African lithosphere.

similar to that of the Central Anatolian Volcanic Province and reach velocities as low as 3.8 km/s beneath Mount Erciyes, the largest Quaternary stratovolcano in the Central Anatolian Volcanic Province (Figs. 9C and 10A). The spatial footprint of these slow mantle shear-wave velocities extends across a much broader region than just the Central Anatolian Volcanic Province, encompassing nearly the entire Central Anatolian Basin, the southern Kirşehir Block, and even the Eastern Taurus Mountains near the Central Anatolian fault zone.

DISCUSSION

A Link between Lithospheric Thickness, Deformation, and Volcanism?

The lithosphere-asthenosphere boundary (LAB) is a rheological boundary between the rigid lithosphere and ductile asthenosphere. In seismic studies, the LAB is generally associated with a gradational decrease in shear-wave velocities corresponding to a decrease in viscosity and possibly a small amount of melt (Eaton et al., 2009; Fischer et al., 2010). In this study, we investigate the character of the upper mantle using two separate approaches to provide evidence (or lack thereof) for the presence of subcontinental mantle lithosphere beneath central Anatolia.

In the first approach, we define the LAB as the depth of the maximum negative velocity gradient after a shear velocity of 4.4 km/s is reached, a velocity that we infer to be representative of lithospheric mantle. The lithospheric thickness of the Anatolian plate was found to be at a relatively constant depth of ~ 80 km based on a recent regional-scale S-wave receiver-function study (Kind et al., 2015); however, at the finer scale resolved in this study, we observe a much more variable lithospheric thickness ranging from <50 km in the Arabian plate to ~ 80 km in the Eastern Taurus Mountains and northern Kirşehir Block (Fig. 11). The thin lithosphere of the Arabian plate in this region is consistent with previous S-wave receiver-function results farther east (Angus et al., 2006). In Figure 11, the white regions indicate that the depth to the LAB is ambiguous due to shear velocities that do not reach our defined cutoff of 4.4 km/s as a proxy for lithospheric mantle (e.g., the Central Anatolian Volcanic Province) or as the result of a nearly monotonically increasing velocity-depth profile such that a negative velocity gradient isn't obtained at a realistic depth for the LAB (e.g., the Central Taurus Mountains). It is important to note that if no mantle lithosphere exists beneath a region, the crust-mantle transition (Moho) would also represent the LAB. In this case, the negative gradient algorithm described above will not be useful in constraining the depth to the LAB, as the transition from crustal to asthenospheric mantle would be a velocity increase (no negative gradient) as opposed to the decrease that we usually associate with the LAB. This may be the case in some of central Anatolia.

Because shear-wave velocities in the uppermost mantle beneath central Anatolia can be very slow (Fig. 10C), the “negative-gradient” approach described above does not return results for the entire region. Thus, to provide evidence for the presence of lithospheric mantle throughout the entire region, we compute the average shear-wave velocity in the top 30 km of the mantle relative to crustal thickness estimates derived from receiver functions (Özacar et al., 2010; Vanacore et al., 2013; Abgami et al., 2017) (Supplemental Fig. S2 [see footnote 1]). We use a lower shear-velocity limit (4.3 km/s) as indicative of the presence of mantle lithosphere in this analysis to allow for uncertainties in crustal thickness estimates (which could incorporate crustal velocities into the mantle average if our estimated crustal thickness is shallower than the true crustal thickness) and the possibility that the lithospheric mantle is <30 km thick (Fig. 12A).

Based on the combination of these two analyses, there is very little evidence for the presence of mantle lithosphere beneath the Central Anatolian Volcanic Province. Thus, this thin to negligible mantle lithosphere allows for hot asthenospheric

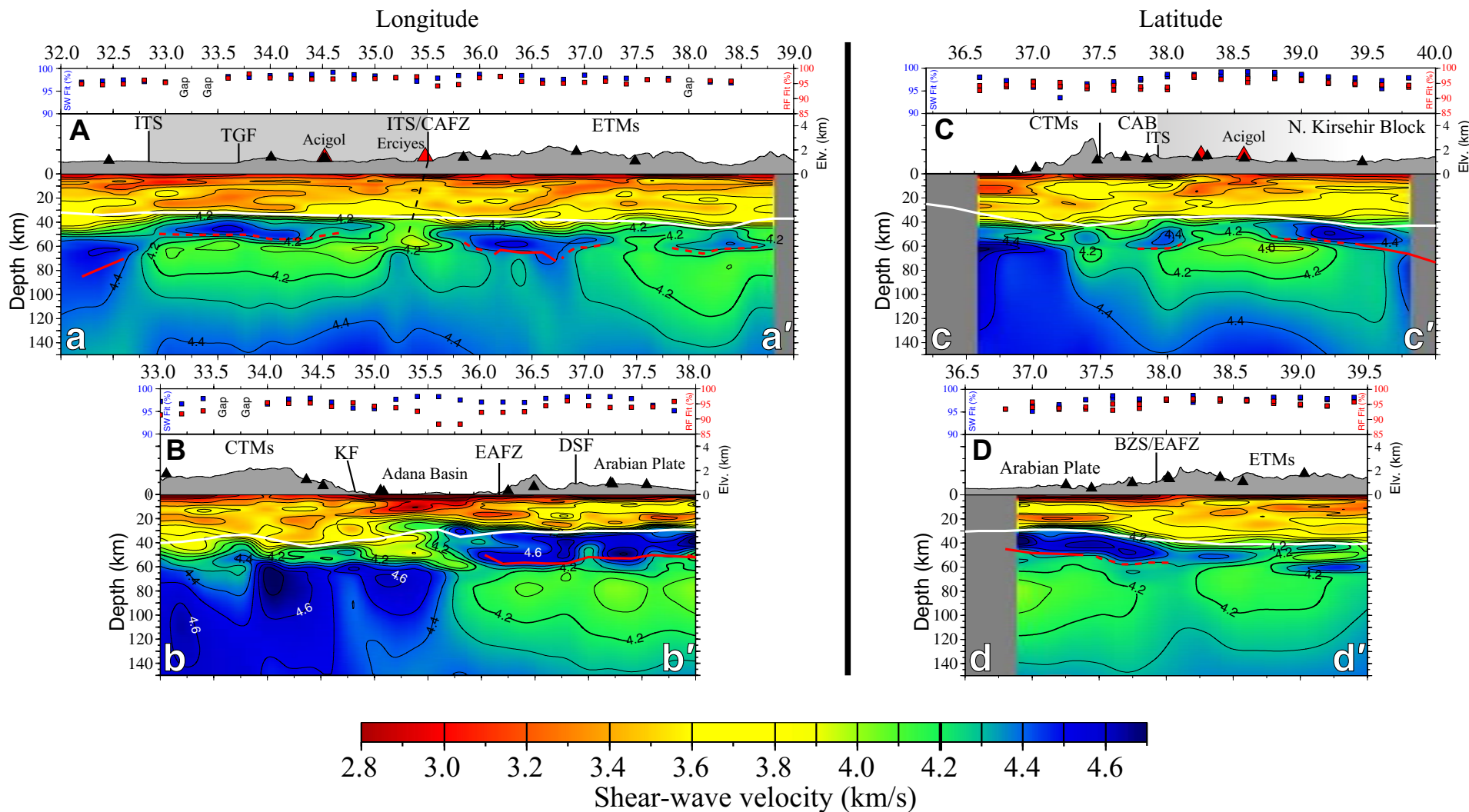
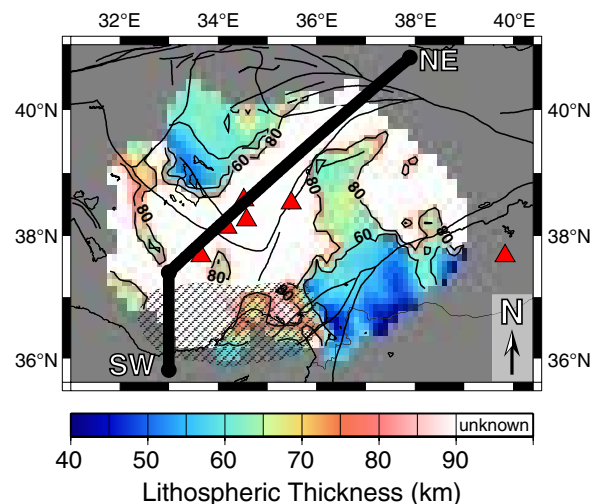


Figure 10. Shear-wave velocity cross sections (locations shown in Fig. 9A) below normalized root-mean-square (NRMS) joint inversion fits to surface-wave dispersion (blue squares) and receiver-function data (red squares). A 100% fit would be a perfect match between observed and predicted data (for map view of NRMS fits, see Supplemental Fig. S3 [footnote 1]). For cross sections: red solid lines are the lithosphere-asthenosphere boundary from negative gradient algorithm (Fig. 11A); red dashed lines are lithosphere-asthenosphere boundary inferred from visual inspection; white lines represent Moho from receiver function analysis (Ozacar et al., 2010; Vanacore et al. 2013; Abgarni et al., 2017); shaded region is southern Kirsehir Block. Contour intervals correspond to vertical black lines in color bar. BZS—Bitlis-Zagros suture; CAB—Central Anatolian Basin; CAFZ—Central Anatolian fault zone; CTMs—Central Taurus Mountains; DSF—Dead Sea fault; EAFZ—East Anatolian fault zone; ETMs—Eastern Taurus Mountains; ITS—Inner-Tauride suture; KF—Kozan fault; TGF—Tuz Gölü fault. (A) The southern Kirsehir Block (shaded region; corresponds to the northern portion of the Central Anatolian Volcanic Province [CAVP]) is underlain by anomalously slow shear velocities in the upper mantle (<4.2 km/s). The slow-velocity upper mantle visible near the downward projection of the ITS may be the subsurface expression of the suture zone. This zone also underlies Mount Erciyes, the largest young stratovolcano in the Central Anatolian Volcanic Province. Thicker lithosphere is observed to the east and west of the ITS outside of the Kirsehir Block (shaded region). (B) Fast upper-mantle shear velocities underlie the CTMs and terminate laterally beneath the Adana Basin. Fast velocities at ~50–60 km depth in the east correspond to the Arabian mantle lithosphere that appears to extend beneath the eastern Adana Basin. This fast upper mantle is underlain by very slow shear-wave velocities. (C) Fast shear-wave velocities in the uppermost mantle beneath the CTMs terminate at the transition to the CAB/CAVP, and give way to very slow shear velocities farther north. (D) We observe no fast-velocity anomalies extending to depths >60 km beneath the easternmost portion of our study area, as slow velocities underlie both the Arabian and Anatolian plates. The fast mantle lithosphere of the Arabian plate appears to terminate near the BZS and EAFZ.

Figure 11. Lithospheric thickness based on depth to the maximum negative shear-wave velocity gradient after a velocity of 4.4 km/s is reached (spatially smoothed over a $0.4^\circ \times 0.4^\circ$ area). White regions show ambiguous results for depth to lithosphere-asthenosphere boundary (LAB) for one of two reasons: (1) Shear velocities of 4.4 km/s are not reached until unrealistic depths to the LAB (Central Anatolian Volcanic Province and Eastern Taurus Mountains); or (2) no significant negative velocity gradient exists (Central Taurus Mountains). Cross-hatched area is where the inferred slab contaminates measurements of lithospheric thickness. Black line shows location of cross section in Fig. 13.



material to come into close proximity with the base of the Central Anatolian crust. Beneath the Central Taurus Mountains, the lithospheric thickness of the overriding plate is difficult to differentiate from the fast, vertically extensive shear velocities associated with the underthrusting African lithosphere (cross-hatched area, Fig. 11). Regardless, the presence of this fast-velocity material would protect the lithosphere of the Central Taurus Mountains from being exposed to asthenospheric material, making the interpretation that the Central Taurus Mountains are supported by shallow asthenosphere unlikely (e.g., Cosentino et al., 2012). Beneath the Arabian plate,

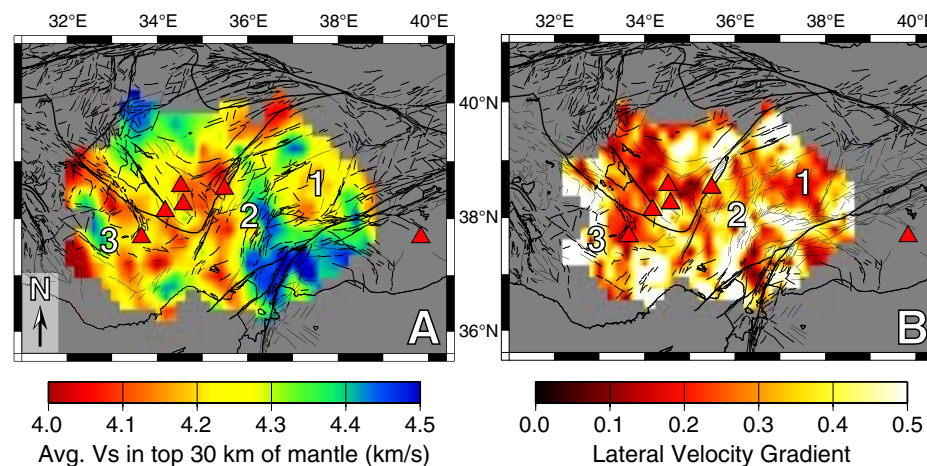


Figure 12. (A) Map of average shear velocities in the upper 30 km of the mantle relative to crustal thickness estimates (Supplemental Fig. S2 [see footnote 1]). Fast shear velocities are a proxy for where lithospheric mantle exists, while slow average velocities indicate either little to no mantle lithosphere (asthenosphere) or very warm mantle lithosphere. (1) Faulting encompasses a zone of slow seismic velocities surrounded by faster mantle lithosphere in the Arabian plate and Eastern Taurus Mountains. (2) A continuous, curved high-velocity gradient correlates well with a curvature in the dominant strike of faulting in the Eastern Taurus Mountains. (3) Southern edge of a NW-SE fast anomaly bounded by faults of similar orientation. (B) Map of the lateral gradient in average shear velocity derived from Figure 11B (units of $\text{km/s}/0.2^\circ$). The rapid transition between fast and slow average shear velocities (lighter colors) seems to correlate well with higher fault densities and volcanics. Numbers correspond to descriptions in Figure 11A and text.

the Eastern Taurus Mountains, and the northwestern Kırşehir Block, there is evidence from both approaches for the presence of a thin and seismically fast lithospheric mantle keel.

The strikes of neotectonic fault zones and structures appear to spatially correlate with boundaries between relatively thick and thin and/or negligible mantle lithosphere as inferred from the lateral gradient of the average upper mantle shear velocities (Fig. 12B). In particular, a semi-circular pattern of faulting is located in the Eastern Taurus Mountains at the boundary between slow and fast average upper-mantle shear velocities (Fig. 12, anomaly 1). Also, the N-S-trending thicker lithospheric mantle of the Eastern Taurus Mountains appears to correlate well with areas that show the highest density of neotectonic faulting (Fig. 12, anomaly 2). A similar pattern can be seen southwest of the Central Anatolian Basin, where NW-SE-striking fault orientations bound a thin zone of faster mantle shear velocities (Fig. 12, anomaly 3). The correlation between neotectonic structures and the transition from relatively thick to thin mantle lithosphere (as inferred from shear velocities) could imply that variations in lithospheric thickness play a crucial role in the location and concentration of deformation. Thus, the thickness of mantle lithosphere in Anatolia could contribute to the strength of the lithosphere as a whole, similar to what has been proposed in the western United States (Levander and Miller, 2012).

The magmatic products of the Central Anatolian Volcanic Province are thought to utilize regional tectonic structures that align with the Central Anatolian fault zone and Tuz Gölü fault (Toprak and Göncöoğlu, 1993; Toprak, 1998) (Fig. 2). As with deformation, volcanism throughout central Anatolia also seems to correlate with the transition between slow and fast upper-mantle velocities. This may be because strain in the crust and upper mantle is concentrated at these boundaries, leading to zones of weakness through which melt from the mantle is able to migrate relatively efficiently. In particular, Mount Erciyes, the largest stratovolcano in the Central Anatolian Volcanic Province, is located near the Inner-Tauride suture at the edge of a step at a releasing bend in the Central Anatolian fault zone (Higgins et al., 2015). The depth

projection of the Inner-Tauride suture corresponds well with ~40 km band of slow velocities that separate the fast upper mantle beneath the northern Kirşehir Block and Eastern Taurus Mountains (Fig. 10A, ITS/CAFZ). Thus, the relict lithospheric weakness associated with the Inner-Tauride suture (and now utilized by the Central Anatolian fault zone) represents an efficient pathway for mantle-derived melt to propagate to the surface, and may control the distribution of volcanism in the Central Anatolian Volcanic Province.

The Central Anatolian Volcanic Province

The very slow (<4.2 km/s) shear velocities observed beneath the Central Anatolian Volcanic Province support previous studies that indicate the presence of a hot upper mantle beneath the region (Gök et al., 2003; Biryol et al., 2011; Mutlu and Karabulut, 2011; Bakırcı et al., 2012; Salaün et al., 2012). The presence of melt beneath the Central Anatolian Volcanic Province is harder to constrain, as the effects of high temperatures versus the presence of melt on shear-wave velocity are difficult to separate. Through the numerical modeling of an upper-mantle system, Hammond and Humphreys (2000) estimated a decrease in shear velocity of ~8% per 1% melt. Assuming the mantle lithosphere and asthenosphere are compositionally similar and that the shear velocities in lithospheric mantle would be 4.5 km/s at typical pressures and temperatures, our shear velocities of ~4.1 km/s suggest a melt percentage of >1% beneath the Central Anatolian Volcanic Province (9% velocity decrease). Alternatively, neglecting the temperature effects and considering only the poroelastic effects of interstitial melts (Yoshino et al., 2005), ~4%–6% melt could be present assuming a peridotitic upper-mantle composition based on geochemical results from basaltic magmas in central Anatolia (Delph et al., 2017; Reid et al., 2017). While the effects imposed by the combination of temperature and melt are not well quantified, recent experimental data on polycrystalline aggregates with analogous characteristics to the mantle olivine + basalt melt system found that it is difficult to obtain shear velocities below ~4.2 km/s without temperatures crossing the solidus and presumably initiating melting (McCarthy et al., 2011). The anomalously slow shear velocities observed in the upper mantle beneath the Central Anatolian Volcanic Province, along with the aforementioned studies on the relationships between seismic velocities and melts, provide strong evidence that the upper mantle beneath central Anatolia likely contains some fraction of melt.

The Cyprean Slab beneath the Central Taurus Mountains

Evidence for the presence of the Cyprean slab below the southern margin of the Anatolian plate is accumulating based on upper-mantle seismic velocities and impedance contrasts beneath the Central Taurus Mountains (Bakırcı et al., 2012; Salaün et al., 2012; Govers and Fichtner, 2016; Abgarmi et al., 2017). The fast (>4.5 km/s) shear-wave velocities below the Central Taurus Mountains observed in this study corroborate this interpretation. Abgarmi et al. (2017) recently proposed that the rapid ~2 km uplift of the Central Taurus Mountains was not due to the influx of as-

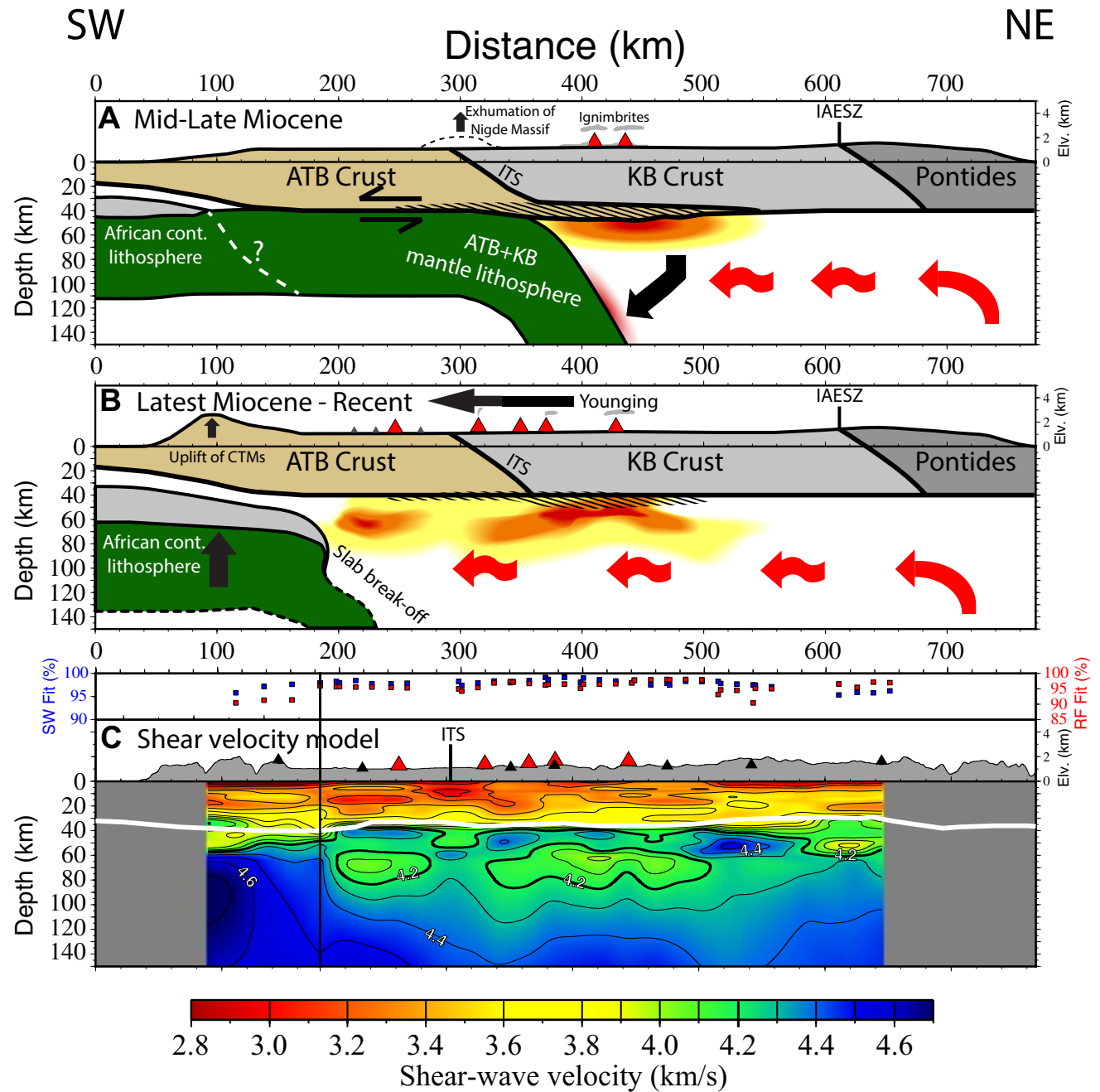
thenosphere beneath the region (Cosentino et al., 2012) but rather slab break-off and subsequent rebound after the detachment of the subducting oceanic lithosphere (Duretz et al., 2011; Schildgen et al., 2014). The removal of this load would allow for the uplift of the Central Taurus Mountains without requiring internal compressional deformation, preserving the near horizontal layering of late Miocene sedimentary rocks (Duretz et al., 2011; Cosentino et al., 2012). Although the appearance of the fast anomaly resolved in this study does not delineate the structure of the subducting slab in detail, it appears that the slab is present until the northern edge of the Central Taurus Mountains near the transition to the Central Anatolian Basin, where it is replaced by very slow shear velocities beneath the Central Anatolian Basin and the Central Anatolian Volcanic Province. To the east, the slab anomaly is replaced with anomalously slow shear-wave velocities in the upper mantle beneath the Adana Basin. These slow velocities appear to merge with the slow and shallow (~60 km) shear-wave velocities beneath the Arabian plate (Fig. 10B). The discontinuous appearance of the fast anomaly along the southern margin of central Anatolia is consistent with the interpretation that the slab is actively deforming and fragmenting, leading to the development of slab tears and gaps (Biryol et al., 2011). The presence of attenuated continental material underthrusting beneath the southern margin of central Anatolia was recently verified by magnetic anomalies (Granot, 2016); thus, this slab deformation may be due to a recent transition from the underthrusting of old Tethyan oceanic lithosphere to the attenuated continental lithosphere of the African passive margin. The underthrusting of continental fragments appears to be common throughout the eastern Mediterranean (Schattner, 2010; Biryol et al., 2011; Delph et al., 2015a; Delph et al., 2015b), with the Anaximander Mountains and Erosthenes Seamount representing un-subducted analogues.

Seismic Velocities and the Evolution of Central Anatolia

While our seismic results only lend insight into the current character of the crust and upper mantle beneath Anatolia, they must be interpreted in light of the recent tectonic history of the region. In Figure 13, we interpret a cross section of our model based on a proposed model for the tectonic history of Central and Eastern Anatolia involving the rollback of a shallow dipping slab initiating in the Miocene (Bartol and Govers, 2014).

During the accretion and transfer of the continental Anatolide-Tauride Block (ATB) and Kirşehir Block (KB) from the downgoing plate to the overriding Eurasian margin, decoupling between their crust and mantle lithosphere may have allowed for the shallow subduction of mantle lithosphere as far north as the Izmir-Ankara-Erzincan suture zone (Bartol and Govers, 2014). Eocene–Oligocene contractional deformation is documented in the Kirşehir and Anatolide-Tauride blocks, indicating a period of compression related to this accretion (Çemen et al., 1999; Gürer et al., 2016). In the Miocene (Fig. 13A), contraction gave way to extension as seen by extensional exhumation in Kirşehir Block, which initiated by at least 17 Ma (Fayon and Whitney, 2007) and the rejuvenation of deposition in the Tuz Gölü basin ca. 11 Ma (Fernandez-Blanco et al., 2013). Voluminous ignimbritic volcanism in the Central Anatolian Volcanic Province also initiated during this time. Felsic-intermediate ignim-

Figure 13. Schematic evolution of central Anatolia since the Miocene following the decoupling of the accreted blocks from their associated mantle lithosphere. ATB—Anatolide-Tauride Block; CTMs—Central Taurus Mountains; ITS—Inner-Tauride suture; IAESZ—Izmir-Ankara-Erzincan suture zone; KB—Kırşehir Block. (A) Mid-late Miocene: Documented extensional exhumation in the Kırşehir Block was driven by rollback of the delaminating Anatolide-Tauride and Kırşehir mantle lithosphere. This delamination allowed hot asthenosphere to rise, melt adiabatically, and come into contact with the base of the crust in central Anatolia, initiating ignimbritic volcanism in the mid-Miocene. (B) Latest Miocene–Recent: Continued rollback of the subducting slab led to the SW migration of the initiation of volcanism. Break-off/necking of the subducting African lithosphere began in the latest Miocene and led to the initiation of uplift in the Central Taurus Mountains due to a reduction in the downgoing slab pull force and isostatic rebound of the subducting continental lithosphere. (C) Shear-wave velocity model along the cross section shown in Figure 11A with normalized root-mean-square joint inversion fits to the surface-wave dispersion (blue squares) and receiver-function data (red squares). Contour intervals correspond to vertical black lines in color bar and white line represents depth to Moho from receiver function analysis.



brites dominate the northern extent of the Central Anatolian Volcanic Province in the Kırşehir Block while smaller mafic-intermediate composition volcanics are more prevalent in the Anatolide-Tauride Block to the south. A possible explanation for this spatial variation in composition is that more felsic material from the underthrusting of some of the Anatolide-Tauride Block's crust beneath the Kırşehir Block along the Inner-Tauride suture was incorporated into mantle melt after slab delamination. Alternatively, the compositional variation may be due to the amount of time that the crust has been exposed to shallow, hot asthenosphere, as volcanism appears to have initiated earlier in the northern Central Anatolian Volcanic Province than in the south. Regardless, exhumation, extension, and volcanism indicate that the delamination of the mantle lithosphere from the accreted terranes initiated by at least mid-Miocene times, presumably foundering to the southwest as indicated by SKS splitting directions in central Anatolia (Paul et al., 2014) and the southwestward younging of the initiation of volcanism (Schleiffarth et al., 2015). This delamination event may also be largely responsible for the thin mantle lithosphere observed beneath most of the Kırşehir and Anatolian-Tauride blocks. As these blocks are thought to have decoupled from their mantle lithosphere during their accretion onto the Eurasian margin (Bartol and Govers, 2014; van Hinsbergen et al., 2016), the majority of the mantle lithosphere associated with these blocks was likely part of the delaminating slab. The removal of the slab led to the influx of asthenospheric mantle to very shallow depths (<50 km) beneath central Anatolia, as seen by the very slow shear-wave velocities imaged in this study.

Along the southern margin of central Anatolia, the initiation of uplift of the Central Taurus Mountains is attributed to slab break-off at ca. 8 Ma (Cosentino et al., 2012; Schildgen et al., 2012; Radeff et al., 2015) (Fig. 13B). This break-off may have been caused by the transition from the subduction of oceanic to continental material at the Cyprean trench. The subduction of this buoyant continental material resulted in the shallow subduction of the African lithosphere as far as the northern margin of the Central Taurus Mountains (Figs. 13B and 13C). Finally, uplift along the Central Taurus Mountains accelerated ca. 1.6 Ma as a result of the arrival of a relatively thicker fragment of continental material (the Eratosthenes Seamount) into the Cyprean trench (Schattner, 2010; Schildgen et al., 2012). An alternative possibility for explaining the late Miocene to recent uplift is the initiation of slab necking ca. 8 Ma caused by the introduction of continental material into the Cyprean trench ca. 8 Ma, followed by complete slab break-off ca. 1.6 Ma which led to the later phase of accelerated uplift in the Central Taurus Mountains.

The possibility of the presence of oceanic lithosphere between the Anatolide-Tauride Block and the African continental margin along the southern margin of central Anatolia, as seen further to the west along the Aegean and westernmost Cyprean trenches and inferred by the presence of ophiolites along the Bitlis-Zagros suture, could make it difficult to invoke a single-slab delamination model. If the lithosphere of the spreading ridge that likely separated the Anatolide-Tauride Block and African plate in the southern branch of the Neotethys was extinct for long enough to become rigid and act as a single plate, then the continuous subduction and subsequent delamination of a single slab throughout Cenozoic may be possible. However, if this was not the case, oceanic subduction could have initiated along the relict lithospheric weakness associated with the spreading ridge, and Fig. 13A could involve

the presence of two slabs: the delaminating slab composed of Anatolide-Tauride and Kırşehir mantle lithosphere (shown in Fig. 13A), and a new slab composed of African lithosphere (not shown). An investigation of the deeper seismic structure interpreted alongside constraints from the surface geology is needed to better infer the Miocene evolution of subduction.

CONCLUSIONS

The CD-CAT seismic deployment, along with the addition of >100 stations from the Kandilli Observatory and Earthquake Research Institute at Boğaziçi University, allows for unprecedented spatial sampling of the crust and upper mantle in central Anatolia. We utilize a recently developed approach to the joint inversion of P-wave receiver functions, ambient noise-derived dispersion data, and earthquake-generated dispersion data to obtain a 3D shear-wave velocity model down to 150 km to understand the interplay between the recent tectonic history of the Central Anatolian plate and the character of subduction along its southern margin.

The main findings of this research are:

1. The thickness of the lithosphere beneath Anatolia is variable but generally thin. Beneath the Arabian plate, Eastern Taurus Mountains, and northwestern Kırşehir Block, lithospheric thickness ranges from ~50–80 km, while very little evidence for mantle lithosphere based on shear-wave velocities is found beneath the Central Anatolian Volcanic Province. As the Kırşehir and Anatolide-Tauride blocks were initially attached to the downgoing plate, most of their mantle lithosphere was most likely removed as part of a Miocene slab delamination event. Gradients in lithospheric thickness also correlate with neotectonic fault density and Miocene to recent volcanism, implying that lithospheric thickness may be playing a crucial role in controlling the distribution of neotectonic structures and volcanism at the surface.
2. The fastest shear-wave velocities in the region are located beneath the Central Taurus Mountains. The presence of these fast velocities provides further evidence that the subducting Cyprean slab underlies the Central Taurus Mountains, which have been uplifted ~2 km in the past 8 m.y. The presence of this seismically fast material makes the interpretation that uplift was driven by the influx of low-density asthenosphere unlikely. Rather, we propose that the majority of the uplift of the Central Taurus Mountains is due to slab rebound after the detachment of the Cyprean slab beneath Anatolia, and we interpret that slab necking/break-off was caused by a transition in the composition of the material arriving at the Cyprean trench from oceanic to attenuated continental in the late Miocene.
3. The fast seismic velocities interpreted as the underthrusting Cyprean slab appear to terminate at the northern margin of the Central Taurus Mountains. These fast velocities give way to a NE-SW trend of very slow upper-mantle shear-wave velocities (<4.2 km/s) that correlate well with the Central Anatolian Volcanic Province. These slow velocities are interpreted to be shallow asthenosphere in which the presence of melt is required. This shallow asthenosphere combined with the lithospheric-scale weakness of the Inner-Tauride suture is

responsible for the distribution of volcanism in the Central Anatolian Volcanic Province. Also, the change in composition of the volcanism in the Central Anatolian Volcanic Province from large volume silicic ignimbrites in the north to smaller mafic to intermediate volcanics in the south, could be due to the melting of highly silicic re-laminated material underthrust beneath the Kirşehir Block. Alternatively, this compositional variation could reflect the amount of time that the overriding plate has been exposed to the hot, shallow asthenosphere.

ACKNOWLEDGMENTS

This research was supported by National Science Foundation grant 1109336. J.R.D. also received support for this project through the Weiss Post-Doctoral Fellowship at Rice University. The authors want to thank Rob Govers and an anonymous reviewer for their helpful comments, which improved this manuscript, as well as the CD-CAT collaborators for useful and insightful discussions. The success of the seismic deployment could not have been accomplished without the assistance of Angela "Mouse" Reusch (The Incorporated Research Institutions for Seismology [IRIS] Portable Array Seismic Studies of the Continental Lithosphere [PASSCAL]) and our Turkish collaborators C. Berk Biryol (University of North Carolina [UNC]), Uğur Teoman (Kandilli Observatory and Earthquake Research Institute [KOERI]), Metin Kahraman (KOERI), Zafer Kaplan (Middle East Technical University), and Savaş Ceylan (Eidgenössische Technische Hochschule Zürich). The authors want to thank Savaş Ceylan for providing a code for surface-wave windowing, as well as Lara Wagner (Carnegie Department of Terrestrial Magnetism) and Sanja Antonijevic (UNC) for providing insight into the two plane-wave tomography codes. The facilities of IRIS Data Services, and specifically the IRIS Data Management Center, were used for access to waveforms and related metadata used in this study. IRIS Data Services are funded through the Seismological Facilities for the Advancement of Geoscience and EarthScope (SAGE) Proposal of the National Science Foundation under Cooperative Agreement EAR-1261681. Waveform data were also obtained from the GeoForschungsZentrum (GFZ) German Research Center for Geosciences and KOERI. The figures in this paper were created using Generic Mapping Tools (GMT; Wessel et al., 2013), and data were analyzed using Seismic Analysis Code (SAC; Goldstein and Snoke, 2005).

REFERENCES CITED

- Abgarmi, B., Delph, J.R., Ozacar, A.A., Beck, S.L., Zandt, G., Sandvol, E., Turkelli, N., and Biryol, C.B., 2017, Structure of the crust and African slab beneath the Central Anatolian Plateau from receiver functions: New insights on isostatic compensation and slab dynamics: *Geosphere*, doi:10.1130/GES01509.1 (in press).
- Angus, D.A., Wilson, D.C., Sandvol, E., and Ni, J.F., 2006, Lithospheric structure of the Arabian and Eurasian collision zone in eastern Turkey from S-wave receiver functions: *Geophysical Journal International*, v. 166, no. 3, p. 1335–1346, doi:10.1111/j.1365-246X.2006.03070.x.
- Ates, A., Kearey, P., and Tufan, S., 1999, New gravity and magnetic anomaly maps of Turkey: *Geophysical Journal International*, v. 136, no. 2, p. 499–502, doi:10.1046/j.1365-246X.1999.00732.x.
- Aydar, E., Schmitt, A.K., Çubukçu, H.E., Akin, L., Ersoy, O., Sen, E., Duncan, R.A., and Atici, G., 2012, Correlation of ignimbrites in the Central Anatolian volcanic province using zircon and plagioclase ages and zircon compositions: *Journal of Volcanology and Geothermal Research*, v. 213–214, p. 83–97, doi:10.1016/j.jvolgeores.2011.11.005.
- Aydin, F., Schmitt, A.K., Siebel, W., Sönmez, M., Ersoy, Y., Lermi, A., Dirik, K., and Duncan, R., 2014, Quaternary bimodal volcanism in the Niğde Volcanic Complex (Cappadocia, Central Anatolia, Turkey): Age, petrogenesis and geodynamic implications: *Contributions to Mineralogy and Petrology*, v. 168, no. 5, p. 1078, doi:10.1007/s00410-014-1078-3.
- Bakırcı, T., Yoshizawa, K., and Özer, M.F., 2012, Three-dimensional S-wave structure of the upper mantle beneath Turkey from surface wave tomography: *Geophysical Journal International*, v. 190, no. 2, p. 1058–1076, doi:10.1111/j.1365-246X.2012.05526.x.
- Barmın, M.P., Ritzwoller, M.H., and Levshin, A.L., 2001, A fast and reliable method for surface wave tomography: *Pure and Applied Geophysics*, v. 158, no. 8, p. 1351–1375, doi:10.1007/PL00001225.

- Bartol, J., and Govers, R., 2014, A single cause for uplift of the Central and Eastern Anatolian plateau?: *Tectonophysics*, v. 637, p. 116–136, doi:10.1016/j.tecto.2014.10.002.
- Bensen, G.D., Ritzwoller, M.H., Barmın, M.P., Levshin, A.L., Lin, F., Moschetti, M.P., Shapiro, N.M., and Yang, Y., 2007, Processing seismic ambient noise data to obtain reliable broad-band surface wave dispersion measurements: *Geophysical Journal International*, v. 169, no. 3, p. 1239–1260, doi:10.1111/j.1365-246X.2007.03374.x.
- Biryol, C.B., Beck, S.L., Zandt, G., and Özacar, A.A., 2011, Segmented African lithosphere beneath the Anatolian region inferred from teleseismic P-wave tomography: *Geophysical Journal International*, v. 184, no. 3, p. 1037–1057, doi:10.1111/j.1365-246X.2010.04910.x.
- Bozkurt, E., 2001, Neotectonics of Turkey—A synthesis: *Geodinamica Acta*, v. 14, no. 1–3, p. 3–30, doi:10.1016/S0985-3111(01)01066-X.
- Boztuğ, D., Jonckheere, R.C., Heizler, M., Ratschbacher, L., Harlavan, Y., and Tichomirova, M., 2009, Timing of post-obduction granitoids from intrusion through cooling to exhumation in Central Anatolia, Turkey: *Tectonophysics*, v. 473, no. 1–2, p. 223–233, doi:10.1016/j.tecto.2008.05.035.
- Bulut, F., Bohnhoff, M., Eken, T., Janssen, C., Kılıç, T., and Dresen, G., 2012, The East Anatolian Fault Zone: Seismotectonic setting and spatiotemporal characteristics of seismicity based on precise earthquake locations: *Journal of Geophysical Research. Solid Earth*, v. 117, B07304, doi:10.1029/2011JB008966.
- Burke, K., and Şengör, C., 1986, Tectonic escape in the evolution of the continental crust, in Barazangi, M., and Brown, L., eds., *Reflection Seismology: The Continental Crust: American Geophysical Union*, p. 41–53, doi:10.1029/GD014p0041.
- Çemen, İ., Göncüoğlu, M.C., and Dirik, K., 1999, Structural Evolution of the Tuzgölü Basin in Central Anatolia, Turkey: *The Journal of Geology*, v. 107, no. 6, p. 693–706, doi:10.1086/314379.
- Cosentino, D., Schildgen, T.F., Cipollari, P., Faranda, C., Gliozzi, E., Hudackova, N., Lucifora, S., and Strecker, M.R., 2012, Late Miocene surface uplift of the southern margin of the Central Anatolian Plateau, Central Taurides, Turkey: *Geological Society of America Bulletin*, v. 124, no. 1–2, p. 133–145, doi:10.1130/B30466.1.
- Delph, J.R., Biryol, C.B., Beck, S.L., Zandt, G., and Ward, K.M., 2015a, Shear wave velocity structure of the Anatolian Plate: Anomalous slow crust in southwestern Turkey: *Geophysical Journal International*, v. 202, no. 1, p. 261–276, doi:10.1093/gji/ggv141.
- Delph, J.R., Zandt, G., and Beck, S.L., 2015b, A new approach to obtaining a 3D shear-wave velocity model of the crust and upper mantle: An application to eastern Turkey: *Tectonophysics*, v. 665, p. 92–100, doi:10.1016/j.tecto.2015.09.031.
- Delph, J.R., Ward, K.M., Zandt, G., Ducea, M.N., and Beck, S.L., 2017, Imaging a magma plumbing system from MASH zone to magma reservoir: *Earth and Planetary Science Letters*, v. 457, p. 313–324, doi:10.1016/j.epsl.2016.10.008.
- Dewey, J.F., Hempton, M.R., Kidd, W.S.F., Saroglu, F., and Şengör, A.M.C., 1986, Shortening of continental lithosphere: The neotectonics of Eastern Anatolia—A young collision zone: *Geological Society of London, Special Publications*, v. 19, no. 1, p. 1–36, doi:10.1144/GSL.SP.1986.019.01.01.
- Dueker, K.G., and Sheehan, A.F., 1997, Mantle discontinuity structure from midpoint stacks of converted P to S waves across the Yellowstone hotspot track: *Journal of Geophysical Research*, v. 102, no. B4, p. 8313, doi:10.1029/96JB03857.
- Duret, T., Gerya, T.V., and May, D.A., 2011, Numerical modelling of spontaneous slab breakoff and subsequent topographic response: *Tectonophysics*, v. 502, no. 1–2, p. 244–256, doi:10.1016/j.tecto.2010.05.024.
- Eaton, D.W., Darbyshire, F., Evans, R.L., Grütter, H., Jones, A.G., and Yuan, X., 2009, The elusive lithosphere-asthenosphere boundary (LAB) beneath cratons: *Lithos*, v. 109, no. 1–2, p. 1–22, doi:10.1016/j.lithos.2008.05.009.
- Fayon, A.K., and Whitney, D.L., 2007, Interpretation of tectonic versus magmatic processes for resetting apatite fission track ages in the Niğde Massif, Turkey: *Tectonophysics*, v. 434, no. 1–4, p. 1–13, doi:10.1016/j.tecto.2007.01.003.
- Fernandez-Blanco, D., Bertotti, G., and Ciner, T.A., 2013, Cenozoic tectonics of the Tuz Gölü Basin (Central Anatolia Plateau, Turkey): *Turkish Journal of Earth Sciences*, v. 22, no. 5, p. 715–738, doi:10.3906/yer-1206-7.
- Fichtner, A., Saygin, E., Taymaz, T., Cupillard, P., Capdeville, Y., and Trampert, J., 2013, The deep structure of the North Anatolian Fault Zone: *Earth and Planetary Science Letters*, v. 373, p. 109–117, doi:10.1016/j.epsl.2013.04.027.
- Fischer, K.M., Ford, H.A., Abt, D.L., and Rychert, C.A., 2010, The Lithosphere-Asthenosphere Boundary: *Annual Review of Earth and Planetary Sciences*, v. 38, no. 1, p. 551–575, doi:10.1146/annurev-earth-040809-152438.

- Forsyth, D.W., and Li, A., 2005, Array analysis of two-dimensional variations in surface wave phase velocity and azimuthal anisotropy in the presence of multipathing interference, *in* Levander, A., and Nolet, G., eds., *Seismic Earth: Array Analysis of Broadband Seismograms*: Washington, D.C., American Geophysical Union, Geophysical Monograph 157, p. 81–98, doi:10.1029/157GM06.
- Gans, C.R., Beck, S.L., Zandt, G., Biryol, C.B., and Ozacar, A.A., 2009, Detecting the limit of slab break-off in central Turkey: New high-resolution Pn tomography results: *Geophysical Journal International*, v. 179, no. 3, p. 1566–1572, doi:10.1111/j.1365-246X.2009.04389.x.
- Gök, R., Sandvol, E., Türkelli, N., Seber, D., and Barazangi, M., 2003, Sn attenuation in the Anatolian and Iranian plateau and surrounding regions: *Geophysical Research Letters*, v. 30, no. 24, p. 1–13, doi:10.1029/2003GL018020.
- Goldstein, P., and Snoke, J.A., 2005, SAC Availability for the IRIS Community: Incorporated Research Institutions for Seismology Newsletter, v. 7, 6 p.
- Govers, R., and Fichtner, A., 2016, Signature of slab fragmentation beneath Anatolia from full-waveform tomography: *Earth and Planetary Science Letters*, v. 450, p. 10–19, doi:10.1016/j.epsl.2016.06.014.
- Granot, R., 2016, Palaeozoic oceanic crust preserved beneath the eastern Mediterranean: *Nature Geoscience*, v. 9, p. 701–705, doi:10.1038/ngeo2784.
- Gürer, D., Hinsbergen, D.J.J., Matenco, L., Corfu, F., and Cascella, A., 2016, Kinematics of a former oceanic plate of the Neotethys revealed by deformation in the Ulukışla basin (Turkey): *Tectonics*, v. 35, p. 2385–2416, doi:10.1002/2016TC004206.
- Hammond, W.C., and Humphreys, E.D., 2000, Upper mantle seismic wave velocity: Effects of realistic partial melt geometries: *Journal of Geophysical Research*, v. 105, no. B5, p. 10,975–10,986, doi:10.1029/2000jb900041.
- Higgins, M., Schoenbohm, L.M., Brocard, G., Kaymakci, N., Gosse, J.C., and Cosca, M.A., 2015, New kinematic and geochronologic evidence for the Quaternary evolution of the Central Anatolian fault zone (CAFZ): *Tectonics*, v. 34, no. 10, p. 2118–2141, doi:10.1002/2015TC003864.
- Jolivet, L., and Faccenna, C., 2000, Mediterranean extension and the Africa-Eurasia collision: *Tectonics*, v. 19, no. 6, p. 1095–1106, doi:10.1029/2000TC900018.
- Julià, J., Ammon, C.J., Herrmann, R.B., and Correig, A.M., 2000, Joint inversion of receiver function and surface wave dispersion observations: *Geophysical Journal International*, v. 143, no. 1, p. 99–112, doi:10.1046/j.1365-246x.2000.00217.x.
- Keskin, M., 2003, Magma generation by slab steepening and breakoff beneath a subduction-accretion complex: An alternative model for collision-related volcanism in Eastern Anatolia, Turkey: *Geophysical Research Letters*, v. 30, no. 24, p. 7–10, doi:10.1029/2003GL018019.
- Kind, R., Eken, T., Tilmann, F., Sodoudi, F., Taymaz, T., Bulut, F., Yuan, X., Can, B., and Schneider, F., 2015, Thickness of the lithosphere beneath Turkey and surroundings from S-receiver functions: *Solid Earth*, v. 6, no. 3, p. 971–984, doi:10.5194/se-6-971-2015.
- Koçyigit, A., and Beyhan, A., 1998, A new intracontinental transcurrent structure: the Central Anatolian Fault Zone, Turkey: *Tectonophysics*, v. 284, no. 3–4, p. 317–336, doi:10.1016/S0040-1951(99)00227-9.
- Le Pennec, J.L., Bourdier, J.L., Froger, J.L., Temel, A., Camus, G., and Gourgaud, A., 1994, Neogene ignimbrites of the Nevşehir plateau (Central Turkey): Stratigraphy, distribution and source constraints: *Journal of Volcanology and Geothermal Research*, v. 63, no. 1–2, p. 59–87, doi:10.1016/0377-0273(94)90018-3.
- Le Pichon, X., and Kreemer, C., 2010, The Miocene-to-Present Kinematic Evolution of the Eastern Mediterranean and Middle East and its implications for dynamics: *Annual Review of Earth and Planetary Sciences*, v. 38, no. 1, p. 323–351, doi:10.1146/annurev-earth-040809-152419.
- Lefebvre, C., Kalijn Peters, M., Wehrens, P.C., Brouwer, F.M., and van Roermond, H.L.M., 2015, Thermal history and extensional exhumation of a high-temperature crystalline complex (Hırkadağ Massif, Central Anatolia): *Lithos*, v. 238, p. 156–173, doi:10.1016/j.lithos.2015.09.021.
- Levander, A., and Miller, M.S., 2012, Evolutionary aspects of lithosphere discontinuity structure in the western U.S.: *Geochemistry, Geophysics, Geosystems*, v. 13, Q0AK07, doi:10.1029/2012GC004056.
- Li, A., 2011, Shear wave model of southern Africa from regional Rayleigh wave tomography with 2-D sensitivity kernels: *Geophysical Journal International*, v. 185, no. 2, p. 832–844, doi:10.1111/j.1365-246X.2011.04971.x.
- Lister, G.S., Forster, M.A., and Rawling, T.J., 2001, Episodicity during orogenesis, *in* Miller, J.A., Holdsworth, R.E., Buick, I.S., and Hand, M., eds., *Continental Reactivation and Reworking*: Geological Society of London Special Publication 184, p. 89–113, doi:10.1144/GSL.SP.2001.184.01.06.
- Luo, Y., Yang, Y., Xu, Y., Xu, H., Zhao, K., and Wang, K., 2015, On the limitations of interstation distances in ambient noise tomography: *Geophysical Journal International*, v. 201, no. 2, p. 652–661, doi:10.1093/gji/ggv043.
- McCarthy, C., Takei, Y., and Hiraga, T., 2011, Experimental study of attenuation and dispersion over a broad frequency range: 2. The universal scaling of polycrystalline materials: *Journal of Geophysical Research*. *Solid Earth*, v. 116, no. 9, p. 1–18, doi:10.1029/2011JB008384.
- Menant, A., Jolivet, L., and Vrielynck, B., 2016, Kinematic reconstructions and magmatic evolution illuminating crustal and mantle dynamics of the eastern Mediterranean region since the late Cretaceous: *Tectonophysics*, v. 675, p. 103–140, doi:10.1016/j.tecto.2016.03.007.
- Mutlu, A.K., and Karabulut, H., 2011, Anisotropic Pn tomography of Turkey and adjacent regions: *Geophysical Journal International*, v. 187, no. 3, p. 1743–1758, doi:10.1111/j.1365-246X.2011.05235.x.
- Okay, A.I., and Tüysüz, O., 1999, Tethyan sutures of northern Turkey: *Geological Society of London, Special Publications*, v. 156, no. 1, p. 475–515, doi:10.1144/GSL.SP.1999.156.01.22.
- Okay, A.I., Zattin, M., and Cavazza, W., 2010, Apatite fission-track data for the Miocene Arabia-Eurasia collision: *Geology*, v. 38, no. 1, p. 35–38, doi:10.1130/G30234.1.
- Özacar, A.A., Zandt, G., Gilbert, H., and Beck, S.L., 2010, Seismic images of crustal variations beneath the East Anatolian Plateau (Turkey) from teleseismic receiver functions: *Geological Society of London, Special Publications*, v. 340, no. 1, p. 485–496, doi:10.1144/SP340.21.
- Özbakir, A.D., Govers, R., and Wortel, R., 2017, Active faults in the Anatolian-Aegean plate boundary region with Nubia: *Turkish Journal of Earth Sciences*, v. 26, p. 30–56, doi:10.3906/yer-1603-4.
- Parlak, O., Karaoğlu, F., Rızaoğlu, T., Klötzli, U., Koller, F., and Billor, Z., 2013, U-Pb and ⁴⁰Ar-³⁹Ar geochronology of the ophiolites and granitoids from the Tauride belt: Implications for the evolution of the Inner Tauride suture: *Journal of Geodynamics*, v. 65, p. 22–37, doi:10.1016/j.jog.2012.06.012.
- Paul, A., Karabulut, H., Mutlu, A.K., and Salaün, G., 2014, A comprehensive and densely sampled map of shear-wave azimuthal anisotropy in the Aegean-Anatolia region: *Earth and Planetary Science Letters*, v. 389, p. 14–22, doi:10.1016/j.epsl.2013.12.019.
- Piromallo, C., and Morelli, A., 2003, P wave tomography of the mantle under the Alpine-Mediterranean area: *Journal of Geophysical Research*. *Solid Earth*, v. 108, no. B2, p. 1–23, doi:10.1029/2002JB001757.
- Radeff, G., Schildgen, T.F., Cosentino, D., Strecker, M.R., Cipollari, P., Darbaş, G., and Gürbüz, K., 2015, Sedimentary evidence for late Messinian uplift of the SE margin of the Central Anatolian Plateau: Adana Basin, southern Turkey: *Basin Research*, v. 29, p. 488–514, doi:10.1111/bre.12159.
- Rau, C.J., and Forsyth, D.W., 2011, Melt in the mantle beneath the amagmatic zone, southern Nevada: *Geology*, v. 39, no. 10, p. 975–978, doi:10.1130/G32179.1.
- Reid, M.R., Schleiffarth, W.K., Cosca, M.A., Delph, J.R., Blichert-Toft, J., and Cooper, K.M., 2017, Shallow melting of MORB-like mantle under hot continental lithosphere, Central Anatolia: *Geochemistry, Geophysics, Geosystems*, v. 18, p. 1866–1888, doi:10.1002/2016GC006772.
- Reilinger, R., McClusky, S., Vernant, P., Lawrence, S., Ergintav, S., Cakmak, R., Ozener, H., Kadirov, F., Guliev, I., Stepanyan, R., Nadariya, M., Hahubia, G., Mahmoud, S., Sakr, K., et al., 2006, GPS constraints on continental deformation in the Africa-Arabia-Eurasia continental collision zone and implications for the dynamics of plate interactions: *Journal of Geophysical Research*. *Solid Earth*, v. 111, B05411, doi:10.1029/2005JB004051.
- Salaün, G., Pedersen, H.A., Paul, A., Farra, V., Karabulut, H., Hatzfeld, D., Papazachos, C., Childs, D.M., and Pequegnat, C., 2012, High-resolution surface wave tomography beneath the Aegean-Anatolia region: Constraints on upper-mantle structure: *Geophysical Journal International*, v. 190, no. 1, p. 406–420, doi:10.1111/j.1365-246X.2012.05483.x.
- Schattner, U., 2010, What triggered the early-to-mid Pleistocene tectonic transition across the entire eastern Mediterranean?: *Earth and Planetary Science Letters*, v. 289, no. 3–4, p. 539–548, doi:10.1016/j.epsl.2009.11.048.
- Schildgen, T.F., Cosentino, D., Bookhagen, B., Niedermann, S., Yildirim, C., Echter, H., Wittmann, H., and Strecker, M.R., 2012, Multi-phased uplift of the southern margin of the Central Anatolian plateau, Turkey: A record of tectonic and upper mantle processes: *Earth and Planetary Science Letters*, v. 317–318, p. 85–95, doi:10.1016/j.epsl.2011.12.003.
- Schildgen, T.F., Yildirim, C., Cosentino, D., and Strecker, M.R., 2014, Linking slab break-off, Hellenic trench retreat, and uplift of the Central and Eastern Anatolian plateaus: *Earth-Science Reviews*, v. 128, p. 147–168, doi:10.1016/j.earscirev.2013.11.006.

- Schleiffarth, W.K., Reid, M.R., and Cosca, M.A., 2015, Ages, distribution, and evolution of Miocene basalts, East-Central Anatolia: Eos (Transactions, American Geophysical Union), Fall Meeting, abstract #T22B-08.
- Şengör, A.M.C., and Yılmaz, Y., 1981, Tethyan evolution of Turkey: A plate tectonic approach: *Tectonophysics*, v. 75, no. 3–4, p. 181–241, doi:10.1016/0040-1951(81)90275-4.
- Şengör, A.M.C., Görür, N., and Saroglu, F., 1985, Strike-slip faulting and related basin formation in zones of tectonic escape: Turkey as a case study: *Society of Economic Paleontologists and Mineralogists, Special Papers*, v. 37, p. 227, doi:10.2110/pec.85.37.0227.
- Şengör, A.M.C., Özeren, S., Genç, T., and Zor, E., 2003, East Anatolian high plateau as a mantle-supported, north-south shortened domal structure: *Geophysical Research Letters*, v. 30, no. 8045, doi:10.1029/2003GL017858.
- Spakman, W., van der Lee, S., and van der Hilst, R., 1993, Travel-time tomography of the European-Mediterranean mantle down to 1400 km: *Physics of the Earth and Planetary Interiors*, v. 79, no. 1–2, p. 3–74, doi:10.1016/0031-9201(93)90142-V.
- Toprak, V., 1998, Vent distribution and its relation to regional tectonics, Cappadocian Volcanics, Turkey: *Journal of Volcanology and Geothermal Research*, v. 85, no. 1–4, p. 55–67, doi:10.1016/S0377-0273(98)00049-3.
- Toprak, V., and Göncüoğlu, M.C., 1993, Tectonic control on the development of the Neogene–Quaternary Central Anatolian Volcanic Province, Turkey: *Geological Journal*, v. 28, no. 3–4, p. 357–369, doi:10.1002/gj.3350280314.
- Vanacore, E.A., Taymaz, T., and Saygin, E., 2013, Moho structure of the Anatolian plate from receiver function analysis: *Geophysical Journal International*, v. 193, no. 1, p. 329–337, doi:10.1093/gji/ggs107.
- van Hinsbergen, D.J.J., Maffione, M., Plunder, A., Kaymakçı, N., Ganerød, M., Hendriks, B.W.H., Corfu, F., Gürer, D., de Gelder, G.I.N.O., Peters, K., McPhee, P.J., Brouwer, F.M., Advokaat, E.L., and Vissers, R.L.M., 2016, Tectonic evolution and paleogeography of the Kirşehir Block and the Central Anatolian Ophiolites, Turkey: *Tectonics*, v. 35, no. 4, p. 983–1014, doi:10.1002/2015TC004018.
- Warren, L.M., Beck, S.L., Biryol, C.B., Zandt, G., Ozacar, A.A., and Yang, Y.J., 2013, Crustal velocity structure of Central and Eastern Turkey from ambient noise tomography: *Geophysical Journal International*, v. 194, no. 3, p. 1941–1954, doi:10.1093/Gji/Ggt210.
- Wessel, P., Smith, W.H.F., Scharroo, R., Luis, J., and Wobbe, F., 2013, Generic Mapping Tools: Improved version released: *Eos (Transactions, American Geophysical Union)*, v. 94, no. 45, p. 409–410, doi:10.1002/2013EO450001.
- Whitney, D.L., and Hamilton, M.A., 2004, Timing of high-grade metamorphism in central Turkey and the assembly of Anatolia: *Journal of the Geological Society of London*, v. 161, no. 5, p. 823–828, doi:10.1144/0016-764903-081.
- Whitney, D.L., Teyssier, C., Dilek, Y., and Fayon, A.K., 2001, Metamorphism of the Central Anatolian Crystalline Complex, Turkey: Influence of orogen-normal collision vs. wrench-dominated tectonics on P-T-t paths: *Journal of Metamorphic Geology*, v. 19, no. 4, p. 411–432, doi:10.1046/j.0263-4929.2001.00319.x.
- Wilson, J.T., 1968, Static or Mobile Earth: The Current Scientific Revolution: *Proceedings of the American Philosophical Society*, v. 112, no. 5, p. 309–320.
- Yang, Y., and Forsyth, D.W., 2006, Regional tomographic inversion of the amplitude and phase of Rayleigh waves with 2-D sensitivity kernels: *Geophysical Journal International*, v. 166, no. 3, p. 1148–1160, doi:10.1109/TIM.2006.876410.
- Yoshino, T., Takei, Y., Wark, D.A., and Watson, E.B., 2005, Grain boundary wetness of texturally equilibrated rocks, with implications for seismic properties of the upper mantle: *Journal of Geophysical Research, B, Solid Earth*, v. 110, no. 8, p. 1–16, doi:10.1029/2004JB003544.
- Zhou, Y., Dahlen, F.A., and Nolet, G., 2004, Three-dimensional sensitivity kernels for surface wave observables: *Geophysical Journal International*, v. 158, no. 1, p. 142–168, doi:10.1111/j.1365-246X.2004.02324.x.